Journal of Hazardous Materials 510 (2026) 142088

Contents lists available at ScienceDirect

Journal of Hazardous Materials

journal homepage: www.elsevier.com/locate/jhazmat

Mechanochemical upcycling of pyrolyzed cork waste into biocompatible superhydrophobic PDMS sponges for passive oil–water separation

Antonella Iaia [a,b,1], Roberta Di Maio [a,b,1], Clara Piccirillo [a], Valeria Garzarelli [a,b,c], Concetta Nobile [a], Alessia Rinaldi [a], Viviana Vergaro [b,c], Elisabetta Primiceri [a,b], Antonio Grieco [d], Maria Serena Chiriacò [a,b], Antonio Turco [a,b,*], Francesco Ferrara [a,b]

[a] CNR Nanotec Institute of Nanotechnology, via per Monteroni, Lecce 73100, Italy
[b] Tecnomed Puglia - Tecnopolo per la medicina di precisione (Biotech Lecce Hub) c/o Campus Ecotekne, via Monteroni, Lecce 73100, Italy
[c] Department of Experimental Medicine, University of Salento, Campus Ecotekne, via per Monteroni, Lecce 73100, Italy
[d] Department of Engineering for Innovation, University of Salento, via per Monteroni, Lecce 73100, Italy

HIGHLIGHTS

- Green upcycling of cork waste into biocompatible PDMS oil-sorbent sponges.
- Solvent-free mechanochemical and microwave route to cork-derived carbon/PDMS sponge.
- > 99% oil removal and high reusability over 100 squeezing regeneration cycles.
- Biocompatible sorbents show no cytotoxicity in direct and indirect cell exposure.
- Effective passive oil–water separation demonstrated in real seawater samples.

GRAPHICAL ABSTRACT

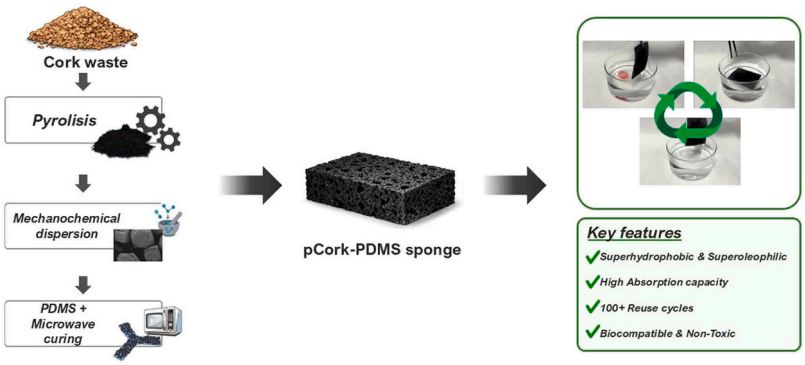

ARTICLE INFO

Keywords:
Oil water remediation
Cork upcycling
Superhydrophobic sponge
Biocompatibility
Mechanochemistry

ABSTRACT

Oil spill pollution and industrial oily wastewater require remediation materials that combine high separation efficiency, mechanical durability, and environmental safety. Here, we report a solvent-free fabrication route for porous pyrolyzed cork–polydimethylsiloxane (pCork–PDMS) composite sponges based on cork-waste pyrolysis, mechanochemical activation processing, NaCl hard templating, and microwave-assisted curing. The optimized composite exhibits superhydrophobic/superoleophilic behavior with a water contact angle (WCA) of 151.7 ± 2.7° and enables passive oil–water separation with ~99% efficiency for both floating and submerged oils. The sponge retained its sorption capacity over 100 sorption–squeezing cycles and maintained mechanical stability under repeated compression. Performance validation in harsh conditions and real seawater confirms operational robustness under realistic environmental conditions. In vitro cytotoxicity assays under both direct and indirect exposure using HaCaT keratinocytes and OECM-1 epithelial cells revealed no significant acute

* Corresponding author at: CNR Nanotec Institute of Nanotechnology, via per Monteroni, Lecce 73100, Italy.
E-mail address: antonio.turco@cnr.it (A. Turco).
[1] These authors contributed equally to this study

https://doi.org/10.1016/j.jhazmat.2026.142088
Received 28 January 2026; Received in revised form 18 March 2026; Accepted 13 April 2026
Available online 15 April 2026

cytotoxic effects under the tested conditions, supporting the preliminary safety assessment of these biomass-derived sorbents for oil–water remediation.

1. Introduction

The increasing global demand for petroleum-derived products continues to generate significant environmental risks associated with oil spills, industrial discharges, and oily wastewater [1,2]. Accidental releases during extraction and transport, as well as improper disposal of oil-containing effluents, represent persistent threats to aquatic ecosystems and human health [3]. These challenges necessitate separation technologies that are efficient, scalable, and environmentally responsible.

Conventional oil–water separation approaches, including coagulation [4], skimming [1,5–8], combustion [6–9], gravity separation [4,10], membrane filtration, and flotation [7,11], often involve high energy consumption, complex infrastructure, or the generation of secondary pollutants [2–6,9,12]. In contrast, sorbent-based technologies relying on porous materials provide a passive and energy-efficient alternative [3]. Three-dimensional (3D) porous structures such as polymeric sponges and aerogels have attracted substantial attention due to their low density, interconnected porosity, and ability to capture oils via capillary forces without external energy input. These porous systems enable spontaneous oil uptake driven by wettability and capillary forces, without requiring external energy. This passive mechanism is particularly attractive for large-scale or emergency scenarios, such as marine oil spills. In such cases, deploying active filtration systems over large aquatic areas is logistically complex and economically demanding [13]. In addition to polymeric sponges, aerogels represent another major class of three-dimensional porous materials widely investigated for oil–water separation due to their extremely high porosity, low density, and tunable surface chemistry. Various carbon-, polymer-, and biomass-derived aerogels have shown high sorption capacities. They also exhibit promising separation efficiencies in laboratory studies [14–21]. However, their practical deployment is often challenged by limited mechanical robustness, structural fragility, and scalability constraints, which can affect long-term operational stability. Recent reviews on PDMS–carbon hybrid sorbents highlight the advantages of elastomeric PDMS composites, including mechanical durability, chemical resistance, and structural integrity compared to fragile ultralight aerogels or purely biomass-derived porous networks. As a result, PDMS-based sponges are widely used for oil–water separation owing to their intrinsic hydrophobicity, flexibility, and ease of regeneration [13]. However, pristine PDMS structures often exhibit limited uptake rates and a trade-off between porosity and mechanical strength [22]. Therefore, to enhance performance, carbon-based fillers such as carbon nanotubes and graphene derivatives have been incorporated into PDMS matrices to improve surface roughness, sorption capacity, and mechanical reinforcement [12,23–26]. Although these nanocarbons can significantly improve separation efficiency, their synthesis frequently requires hazardous reagents, multistep purification, and high energy input, raising concerns regarding scalability, environmental footprint, and safe deployment [13].

Biomass-derived carbons obtained via pyrolysis of plant waste provide a potentially more sustainable alternative. Cork, the bark of *Quercus suber* L., is a renewable material harvested without damaging the tree, and its industrial processing generates substantial amounts of fine powder waste. Native cork possesses a hierarchical cellular architecture characterized by closed hexagonal cells with typical dimensions on the order of tens of micrometers and submicrometric channels within the cell walls [27]. Several studies have explored cork-based materials for oil–water separation using different strategies. For example, surface-functionalized cork membranes have been reported to selectively separate oil and water through gravity-driven filtration, relying on the native cellular channels of the cork structure [28,29]. However, these systems typically require continuous flow through a membrane and the use of chemical surface treatments involving fluorinated silanes or solvent-based processes. Other approaches have employed chemically modified cork structures or hybrid coatings to enhance wettability control [30]. While these studies demonstrate the potential of cork as a separation substrate, they generally preserve the native cork architecture and operate through filtration mechanisms rather than capillary-driven sorption.

Pyrolysis converts this biomass into a graphitic carbon framework while preserving aspects of its porous morphology [31]. Moreover, pyrolyzed cork powder has been incorporated into polymeric matrices to impart functional properties; for example, its integration into chitosan scaffolds enhanced electrical conductivity and bioactivity [32].

Cork-derived materials have been investigated as granulated adsorbents for pollutant removal, including antibiotics [33], dyes [34] and oil spills [35]. Carbon-based pyrolysed cork powder was also employed for liquid adsorption processes [36]. Nevertheless, most cork-based systems remain in powder or granular form, which poses limitations in large-scale recovery and reuse. Embedding biomass-derived carbon into a mechanically robust polymeric matrix therefore represents a more viable strategy for operational oil–water remediation.

A key challenge in preparing polymer/carbon composites from pyrolyzed biomass lies in achieving homogeneous dispersion and controlled particle size without altering the carbon surface chemistry. Mechanochemical processing has emerged as a solvent-free approach capable of reducing agglomeration and promoting uniform distribution of carbon fillers within host matrices [37–39]. While mechanochemistry has been extensively applied to synthetic nanocarbons, its use as a post-pyrolysis treatment to engineer biomass-derived graphitic carbon for integration into 3D polymeric scaffolds remains largely unexplored.

In this study, we develop a solvent-free, microwave-assisted fabrication strategy for porous pCork–PDMS composite sponges by integrating cork-waste pyrolysis, mechanochemical processing, NaCl hard templating, and rapid PDMS curing. This approach enables uniform dispersion of pyrolyzed cork particles within an open-cell PDMS framework while preserving the carbon chemical structure. The resulting composites exhibit superhydrophobic/superoleophilic behavior, high oil sorption efficiency, and strong mechanical durability under repeated regeneration. Their performance was also validated in real seawater. In addition, preliminary *in vitro* safety assessment under both direct and indirect exposure conditions was performed to complement the evaluation of separation performance.

2. Experimental section

2.1. Materials and chemicals

In this study, Sylgard 184 kit (PDMS) was purchased from Dow-Corning and prepared by mixing base and curing agent in a 10:1 ratio. Cork waste powder was supplied by Amorim Cork Composite (Mozelos, PT), pump oil (Ultragrade Performance 19) was provided by Edwards, vegetable oil was commercial extra virgin olive oil and all other reagents, oils and solvents were acquired from Merck. Ultrapure water (18.1 MΩ·cm^{-1}) was used throughout the experiments, and all solutions were freshly prepared.

The cell lines used in this study were OECM-1 (human oral squamous carcinoma, SCC180, Sigma-Aldrich) and HaCaT (human keratinocytes, Sigma-Aldrich). OECM-1 cells were cultured in Roswell Park Memorial Institute 1640 (RPMI 1640, Corning, 15040CV) medium supplemented with 10% fetal bovine serum (FBS, Sigma-Aldrich, F7524), 1%

penicillin-streptomycin (Sigma-Aldrich, P0781), 1% sodium pyruvate (Sigma-Aldrich, S8636), and 1% glutamine (Sigma-Aldrich, G7513). The HaCaT cell line was cultured in Dulbecco's Modified Eagle's Medium (DMEM, Sigma-Aldrich, 51435 C), supplemented as described for RPMI.

The phosphate-buffered saline (PBS, P4417), 3-(4,5-dimethylthiazol-2-yl)-2,5-diphenyltetrazolium bromide (MTT, M2128) and 4',6-diamidino-2-phenylindole (DAPI, D9542) compounds were purchased from Sigma-Aldrich Company.

2.2. Synthesis of pyrolyzed cork from waste biomass

Pyrolyzed cork was prepared by adapting a previously developed procedure [40]. The cork waste particles exhibited an average size distribution of about 300–400 μm. Prior to utilization, the material was subjected to hot-water treatment at 100°C, a conventional industrial procedure intended to promote a homogeneous and structurally regular morphology. The cork powder was subsequently placed in graphite crucibles and pyrolyzed in a Nabertherm RHTH 120–600/16 high-temperature tube furnace with a horizontal configuration. Before thermal treatment, a high vacuum was established using a turbomolecular pump. The system was then brought back to atmospheric pressure under nitrogen, which was continuously supplied as an inert atmosphere during the process.

The pyrolysis protocol comprised: (i) heating from room temperature to 700°C at a rate of 3°C min^{-1} ; (ii) further heating from 700°C to 900°C at 1°C min^{-1} ; and (iii) an isothermal stage of 30 min at 900°C. The furnace was subsequently cooled to room temperature under natural conditions. The resulting pyrolyzed cork material displayed a completely black appearance. These experimental parameters were selected based on prior studies on cork pyrolysis, which showed that pyrolysis above 700 °C promotes the development of graphitic domains in cork-derived carbon.

2.3. Preparation of pCork-PDMS sponges

The fabrication process is based on a sacrificial salt-templating strategy. Sodium chloride (NaCl) crystals were first used as a removable solid template to define the macroporous architecture of the final sponge. For a representative specimen (1.5 × 1.5 × 0.5 cm^3), 2 g of NaCl crystals were employed as the structural template. The amount of pCork was fixed at 2 wt% with respect to the NaCl template (unless otherwise specified) and was mechanically mixed with NaCl crystals under dry conditions for 24 h at 80 rpm to promote homogeneous distribution of the carbon particles onto the salt surface through non-covalent interactions. At this stage, the mixture forms a dense, non-porous composite powder in which NaCl acts exclusively as a structural template.

A small amount of ultrapure water (8 wt% relative to the total weight of the mixture) was subsequently added to facilitate compaction of the mixture into defined molds, forming a consolidated pCork/NaCl monolith. After drying at 150°C for 1 h to remove residual moisture, the compact was infiltrated with liquid PDMS precursor under reduced pressure to ensure uniform penetration of the polymer phase throughout the interstitial spaces between the salt particles.

Microwave irradiation (350 W) was applied for 10 min to induce rapid PDMS crosslinking. After polymerization, the NaCl template was removed by extensive water washing. This step generated an interconnected open-cell PDMS structure with embedded pCork particles. The final porosity is therefore determined by the salt crystal size and only emerges after template dissolution.

2.4. Characterization of pCork-PDMS sponges

The hydrophobicity of the sponges was evaluated by contact angle measurements using a CAM 200 instrument (KSV Instruments Ltd., Finland) equipped with an automatic liquid dispenser and a high-resolution camera. A 5 μL droplet of ultrapure water was placed on the surface of the material, and the contact angle was determined from the acquired images. Additional image analysis was performed using ImageJ software.

The morphological and surface features of the pCork–PDMS composites were characterized by scanning electron microscopy (SEM) using a high-resolution Field Emission SEM (SIGMA 300VP, Carl ZEISS GmbH, Germany) equipped with GEMINI® technology, an Inlens/SE detector for secondary electrons, and an HBSD detector for backscattered electrons. Measurements were carried out under both high-vacuum and variable-pressure conditions, the latter using nitrogen as the imaging gas to observe non-conductive or beam-sensitive samples. The specimens were fixed to aluminum stubs with double-sided conductive carbon tape before being transferred into the chamber. SEM images were collected using the backscattered electron detector at an accelerating voltage of 20 kV, under 50 Pa nitrogen pressure, with short image integration times to minimize charging and sample damage. The pore size distribution was quantified from SEM cross-sectional images using ImageJ software by measuring the equivalent circular diameter of 100 randomly selected pores.

The structural porosity of the pCork–PDMS sponges was estimated from the bulk density of the material using the relationship between the apparent density of the porous solid and the density of the non-porous polymer phase. The porosity (ϕ) can be approximated as:

$$\phi = 1 - \frac{\rho_{sponge}}{\rho_{solid}} \quad (1)$$

Where ρ_{sponge} is the bulk density of the porous sponge and ρ_{solid} is the density of the dense polymer matrix. Instead, the apparent porosity was estimated as:

$$\phi_{app} = \frac{m_{solvent}}{\rho_{solvent} V_{sponge}} \quad (2)$$

Where $m_{solvent}$ is the sorbed solvent mass and $\rho_{solvent}$ is the solvent density and V_{sponge} is the geometrical volume of the sponge.

Raman spectroscopy was performed on a WITec alpha300R confocal Raman microscope equipped with a 633 nm laser, with measurements conducted on solid samples deposited on glass coverslips. Thermogravimetric analysis (TGA) was carried out using a TGA SDT Q600 instrument (TA Instruments, New Castle, DE, USA) under nitrogen atmosphere. Approximately 20 mg of each sample was tested, starting with an isothermal step at 100 °C for 20 min to remove adsorbed moisture, followed by a temperature ramp from 100 °C to 700 °C at a rate of 10 °C min^{-1} to evaluate weight loss and thermal stability.

Fourier transform infrared (FT-IR) spectroscopy was performed using a Shimadzu IRXross spectrophotometer equipped with an attenuated total reflectance (ATR) accessory to identify the functional groups. Spectra were collected in the range 4000–400 cm^{-1} with a resolution of 4 cm^{-1}, and 50 scans were accumulated for each measurement.

Specific surface area (S_{BET}) of pCork, PDMS sponge and pCork-PDMS sponge was evaluated from N_2 adsorption isotherms using a Micrometrics Gemini VII 2390 instrument. N_2 adsorption measurements were carried out at 77 K. Before the analysis, samples were outgassed at 90°C for at least 2 h to remove physisorbed molecules. The S_{BET} was calculated by applying the Brunauer-Emmett-Teller (BET) method from the linear region of the BET plot in the relative pressure (P/P_0) range of 0.05–0.30.

Compressive tests under uniaxial loading were conducted on a ZwickiLine universal testing machine (ZwickRoell, Kennesaw, GA, USA) fitted with a 5 kN load cell. Test specimens measured 15 mm × 15 mm in cross-section with a 6 mm height. Compression occurred between parallel platens at ambient temperature. Cyclic loading was applied to 60% strain over 100 cycles to evaluate fatigue resistance under repeated loading. Maximum stress at 60% strain was determined from the initial loading curve, while mechanical retention was quantified by comparing

stress values at 60% strain between cycle 1 and cycle 100.

2.5. Oil sorption, reusability and separation performances of pCork-PDMS sponges

A piece of pCork-PDMS sponge was dipped for 15 min in oil (10 ml). Afterwards, the sample was carefully taken out from the oil bath and immediately weighed to determine the oil mass sorption capacity (M_{abs}) and volume sorption capacity (V_{abs}) by using the following equation:

$$M_{abs} = \frac{m - m_0}{m_0} \tag{3}$$

$$V_{abs} = \frac{(m - m_0)\rho_0}{\rho\, m_0} \tag{4}$$

Where m_0 is the pCork-PDMS initial weight and m is the pCork-PDMS weight after sorption, ρ_0 and ρ are the densities of the absorbent material and the absorbed oil respectively. Repeated oil sorption–desorption cycles were performed to evaluate the reusability of the sponge. Each cycle consisted of immersing the sample in oil for 15 min to achieve sorption equilibrium, followed by weighing to determine the oil sorption capacity. The sample was then manually squeezed and dried in an oven at 60°C before the next cycle. For each tested liquid, sorption measurements were performed in triplicate on independently treated samples. In addition, long-term reusability was evaluated separately through 100 sorption–desorption cycles using the selected model oil.

The oil–water separation capability of the pCork–PDMS composite was further examined by calculating the separation efficiency (η), defined as:

$$\eta = \frac{M_b}{M_a} * 100 \tag{5}$$

where $M_a$is the weight of oil before separation [g], and $M_b$is the weight of oil after separation [g]. This evaluation was conducted for both distilled water–oil mixtures and seawater–oil mixtures, in order to assess the potential applicability of the material under realistic environmental conditions.

The real sea water sample for separation test was obtained from San Cataldo, located 10 km East of the town of Lecce and has a salinity of 37.58‰. The seawater sample was used without further purification and contained typical marine ionic composition

2.6. Biocompatibility assessment

To assess the biocompatibility of the materials developed in the present paper, an MTT assay was performed on cells derived from oral cancer (OECM-1) and normal skin (keratinocytes-HaCaT).

The key chemical component of MTT assay is 3-[4,5-dimethylthiazol-2-yl]-2,5-diphenyl tetrazolium bromide. Viable cells are able to metabolize the tetrazolium compound, thanks to mitochondrial dehydrogenases, producing the insoluble purple MTT formazan crystals.

OECM-1 cells were cultivated in RPMI-1640 culture medium supplemented with 10% FBS, 1% glutamine, 1% sodium pyruvate, and 1% penicillin and streptomycin, while HaCaT cells were cultivated in DMEM culture medium supplemented with the same compounds.

OECM-1 and HaCaT cells were seeded in a 24-well plate separately, at a density of 1.5×10^5 cells per well in 500 µL of culture medium and incubated at 37°C in a humidified atmosphere with 5% CO_2. After cell adhesion, conditioned culture medium was replaced in the culture wells. This was obtained from the 24-hours incubation of culture media with 100 µg/ml and 1 mg/ml of PDMS and PDMS-pCORK sponges in separate wells. A control experiment included untreated cells to establish baseline viability.

For viability assay, 0.5 mg/ml of tetrazolium bromide was dissolved in a complete culture medium. The culture medium was removed from cells and 500 µL of MTT solution was added to each well. After 3 h of incubation at 37°C in a humidified atmosphere with 5% CO_2, the MTT solution was carefully removed and 200 µL of a 2-propanol based solution was added to each well to solubilize the formazan crystals.

The absorbance at 570 nm was measured using a Microplate Reader CLARIOstar PLUS.

The number of viable cells is directly related to the absorbance values, which allows for the calculation of cell viability percentages. This percentage was calculated applying the following formula:

$$Cell\ Viability \quad \% = \frac{Absorbance\ of\ treated\ cells}{Absorbance\ of\ control\ cells} * 100 \tag{6}$$

Furthermore, cellular growth on PDMS sponges and pCORK-PDMS sponges was tested using confocal microscopy. Specifically, the sponges were placed into 24-well cell culture plates after being sterilized with UV light for 30 min. OECM-1 and HaCaT cells were detached from T25 flasks, counted, and then plated at a density of 2×104 on the sponges' surfaces separately. After 3 days, the cells were characterized by an immunofluorescence assay. For this assay, samples were washed three times with PBS and then fixed with 4% paraformaldehyde for 30 min at room temperature. After a washing step, the cells were incubated in 4',6-diamidino-2-phenylindole (DAPI) solution at a final concentration of 1 µg/ml to stain the nuclei. The sponges were then washed in PBS and placed in µ-Slide 8 well ibiTreat (Ibidi Cat. No: 80826) before confocal microscopy analysis using a ZEISS LSM 780 confocal laser scanning microscope with ZEN imaging software (Zeiss, Germany).

3. Results and discussion

3.1. Sustainable fabrication and morphological characterization of cork-derived carbon/PDMS sponges

The composite sponges were fabricated through a salt-templating route in which NaCl crystals act as a sacrificial structural template. The three consecutive steps to produce the composite are summarized in Fig. 1. After pyrolysis, pyrolyzed cork (pCork) powder was first distributed onto the NaCl surface to ensure homogeneous carbon dispersion prior to polymer infiltration through non-covalent mechanochemical approach [41]. It is important to note that this initial pCork/NaCl compact is not porous; rather, it constitutes a dense monolith in which salt particles define the future pore architecture. Porosity is generated only after PDMS infiltration, microwave-induced crosslinking, and subsequent NaCl removal by water washing.

This sequence ensures that the final open-cell structure reflects the salt particle size while maintaining uniform embedding of pCork within the PDMS matrix. More in detail, cork powder, an abundant byproduct of the cork stopper industry (about 400 µm), was selected for its renewable origin and widespread availability, representing a sustainable alternative to synthetic or fossil-based carbon fillers. The cork powder underwent high-temperature pyrolysis under inert conditions to induce graphitization (Fig. 1a), as verified by Raman spectroscopy through the appearance of prominent D (~1350 cm^{-1}) and G (~1580 cm^{-1}) bands (Fig. 2h). These features are consistent with the formation of a partially ordered sp^2 carbon structure and confirm the successful conversion of the biomass into pyrolyzed material with graphitic domains. Following pyrolysis, the resulting carbon material retains the characteristic cellular morphology of cork, displaying a three-dimensional network of pores that reflects the original anisotropic structure of the plant tissue (Fig. 1b; Figure S1).

Following pyrolysis, the carbon powder was subjected to post-pyrolysis non-covalent mechanochemical processing, adapting a strategy previously developed for synthetic nanocarbon systems [38,39]. In the present system, the mechanochemical step does not promote covalent chemical transformation. Instead, it induces fragmentation of pCork agglomerates and favors adsorption of the carbon particles onto the NaCl surface through mechanically assisted non-covalent interactions

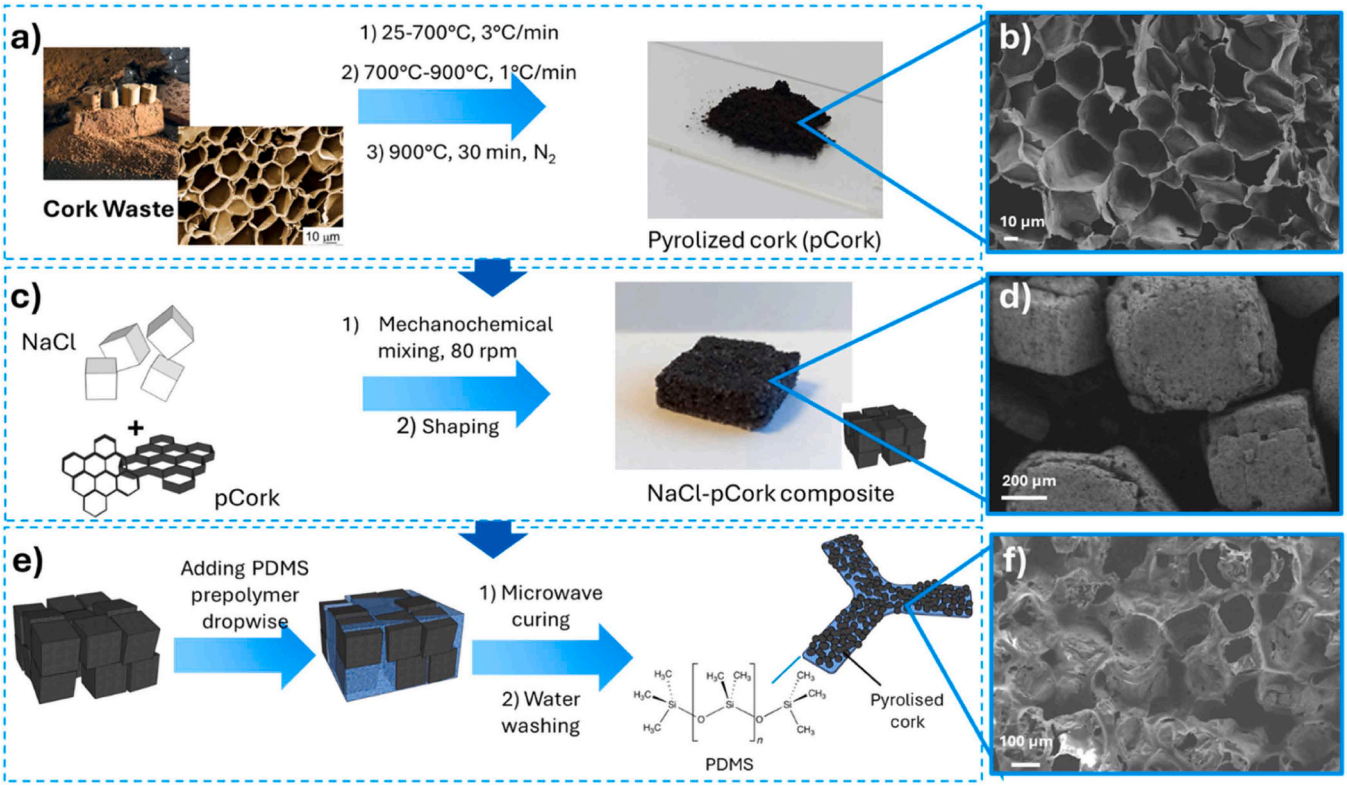

Fig. 1. Main steps involved in the preparation of the cork-based composites. Panels (a), (c), and (e) show the schematic workflows of cork pyrolysis, NaCl-templated composite fabrication, and PDMS-based composite synthesis, respectively. The corresponding SEM images acquired after each step are shown in panels (b), (d), and (f): pyrolyzed cork in (b), pCork adsorbed on the NaCl template in (d), and the final pCork–PDMS composite in (f).

[41]. More in detail, pCork was dispersed and adsorbed on NaCl surface by mechanical mixing between the two powders. This solvent-free, energy-efficient approach enabled size reduction and homogeneous dispersion of the insoluble carbon within the salt template. In particular, careful control of the mechanochemical mixing step between pyrolyzed cork and NaCl particles proved crucial in disrupting strong π–π interactions among the pyrolyzed cork domains. This energetic mixing fragmented large agglomerates into smaller, more uniform particles. As a result, cork-derived carbon was evenly distributed on the NaCl surface through non-covalent interactions (Fig. 1d and Supporting S2 a-c). This improved accessibility and facilitated its incorporation during sponge fabrication (Fig. 1c). Notably, this dry mechanochemical method eliminates the need for wet chemical dispersion processes and hazardous organic solvents. These conventional approaches are commonly used to achieve homogeneous carbon dispersion but often alter surface chemistry and reduce environmental compatibility. As demonstrated by Raman spectroscopy (Figure S2d), the pristine surface composition of the cork-derived carbon is fully preserved; this is further confirmed by the unchanged D/G band ratio observed for pCork adsorbed on NaCl compared with pristine pCork. At the same time, a fine, stable, and uniform dispersion of pCork within the templating matrix is evidenced by SEM characterization (Figure S2a-c).

Composites were prepared with varying carbon loadings (1, 2, and 3 wt% with respect to the NaCl template), allowing the evaluation of structure–property relationships and the effect of carbon content on materials fabrication and properties. After the mechanochemical activation mixing of the pyrolyzed cork with NaCl particles, a small amount of water was added to the mixture. This step played a key role in promoting a more effective packing and slight pre-agglomeration of the components, facilitating subsequent molding. The moistened blend was gently pressed into molds of defined shape and dried to ensure the formation of solid monolithic pre-composites and the complete removal of residual moisture (Fig. 1c). Once dried, the porous pCork/NaCl template was impregnated with a PDMS solution, ensuring thorough infiltration of the polymer precursor throughout the template structure. The resulting assembly was then subjected to microwave irradiation, triggering rapid and uniform polymerization of the PDMS phase (Fig. 1e). Notably, the cork-derived carbon significantly enhanced the microwave absorption efficiency in all tested formulations, enabling complete PDMS polymerization at a power of just 350 W—substantially lower than the 900 W required for sponges composed of PDMS alone. This effect is illustrated in Figure S3, where optical and infrared images compare pure NaCl and NaCl–pCork samples before and after microwave treatment. While the NaCl template shows low heating under microwave irradiation, the NaCl–pCork composite exhibits a pronounced temperature increase, reaching approximately 150–160 °C after irradiation at 350 W. Such temperatures are sufficient to ensure the complete crosslinking and curing of the infiltrated PDMS, confirming the crucial role of the cork-derived carbon as an efficient microwave absorber that promotes localized heating within the templated scaffold. This selective heating enables a microwave-assisted fabrication strategy, allowing rapid PDMS polymerization directly within the templated scaffold while operating at significantly lower microwave power compared with conventional thermal curing.

This result highlights the dual role of the biochar filler as both a structural component and a microwave-activatable agent; this is in agreement with literature, as the good microwave absorbing properties of cork-derived carbon were previously reported [42]. Similar to other graphitic forms of carbon [43], pyrolyzed cork acts as an antenna, efficiently converting microwave radiation into thermal energy and enabling rapid polymerization of PDMS. This property is particularly advantageous for the fast production of oil-absorbing materials, especially in emergency scenarios [44]. Finally, the composites were washed in water to remove NaCl. After removal of the NaCl template by water washing, an interconnected porous composite composed of pCork particles embedded within a PDMS framework is obtained (Fig. 1 f and S4).

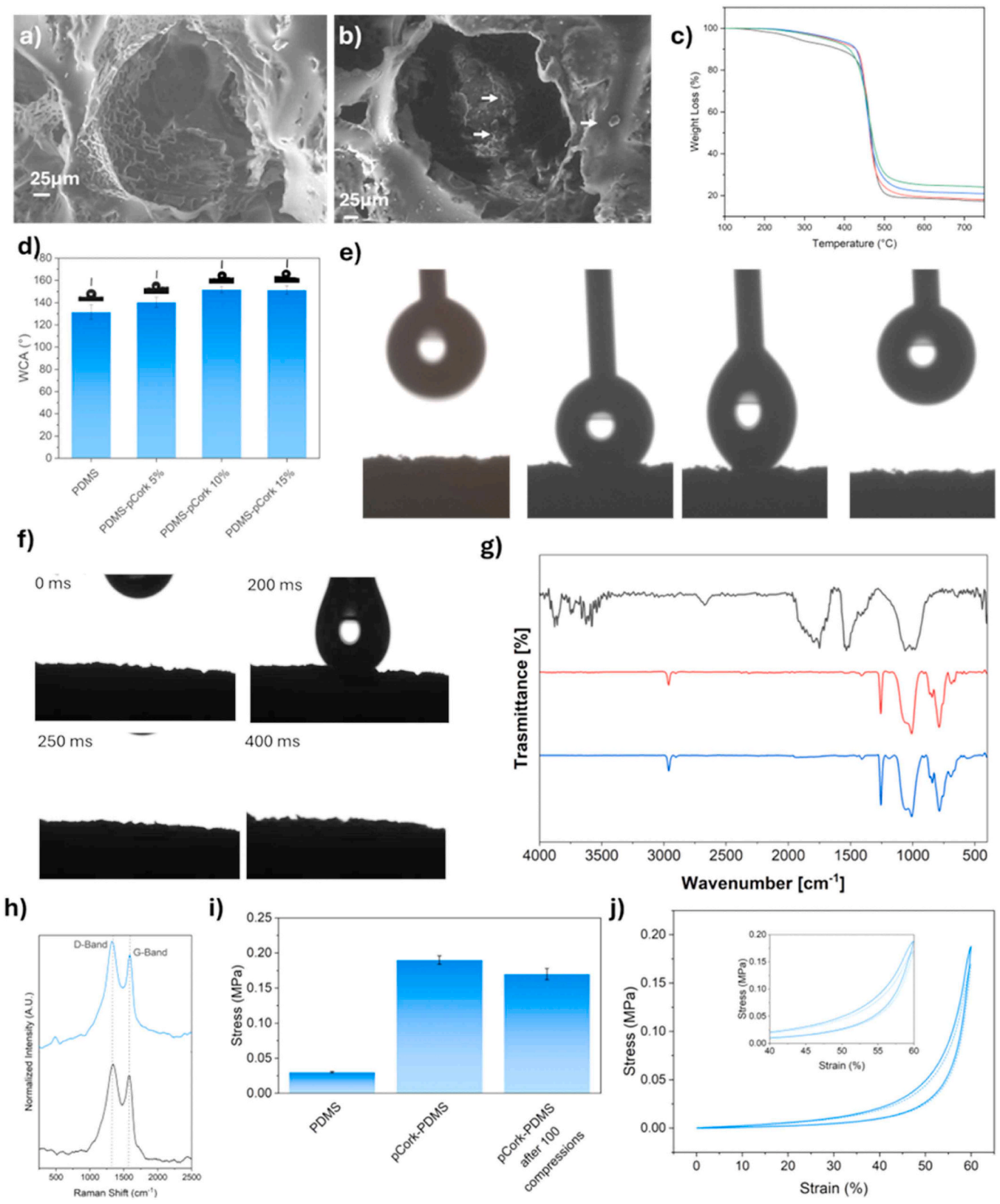

Fig. 2. Scanning electron microscopy (SEM) images of PDMS(a) and pCork-PDMS composites (b). (c) Thermogravimetric analysis (TGA) curves in nitrogen representing weight loss as a function of temperature for PDMS (black curve); 5% pCork-PDMS (red curve); 10% pCork-PDMS (blue curve) and 15% pCork-PDMS (green curve) sponges. (d) Static WCA measurements for pCork-PDMS-based composites with various cork contents. (e) Representative images of dynamic contact angle measurements for water (f) and oil (ethyl acetate). (g) Infrared spectra of pCork (black curve), PDMS (red curve) and pCork-PDMS composite (blue curve) (h) Raman spectra of pCork (black curve) and pCork-PDMS materials (blue curve), showing the D and G bands characteristic of graphitic structures. In i) Stress at 60% strain recorded for different materials. In j) Compressive stress–strain curves measured on pCork-PDMS sponge during cyclic compression (maximum strain = 60%), reporting the 1st (solid line) and 100th cycles (dot line).

The pore size distribution of the final sponge closely mirrors the size distribution of the NaCl template particles. Quantitative image analysis confirms a strong overlap between the two distributions, demonstrating that the macroporosity of the composite originates exclusively from the sacrificial salt template (Figure S4d).

3.2. Chemical characterization and properties of pCork-PDMS sponges

Scanning electron microscopy of PDMS and PDMS/cork sponges confirms that the cork-derived carbon was visibly embedded along the inner surfaces of the pores, with no significant agglomeration or phase separation, indicating high compatibility with the PDMS matrix (Fig. 2a, b and Figure S4). The pCork morphology in the sponge differed significantly from that of pristine cork, which is typically characterized by a honeycomb structure; this confirms that mechanochemical activation steps yielded discrete carbon particles rather than cell-like frameworks, enabling processability and integration into the composite. Moreover, the successful removal of the NaCl template and the absence of residual crystals in SEM cross-sections (Figure S4a-c) confirm the presence of an interconnected macroporous structure

Raman spectroscopy of the composite sponges confirmed that the cork-derived carbon retained its chemical identity throughout the fabrication process, with no detectable degradation of chemical bonds or structural oxidation (Fig. 2h). Notably, comparison of the D and G band intensities between the powdered pCork and the pCork-PDMS composite revealed no significant changes in the D/G intensity ratio, nor an increase in the D band. This indicates that no additional defects were introduced during composite formation and polymer crosslinking; this suggests that, when finely fragmented, the initial carbon structure remains chemically unaltered and robust under microwave-assisted conditions.

The FT-IR spectra of pCork, PDMS sponge and pCork-PDMS composite are shown in Fig. 2g. The analysis allows for the identification of the functional groups and for the possible evaluation of chemical interactions between pCork and the PDMS matrix after composite formation. The spectrum of pCork exhibits several bands associated with oxygen-containing functional groups typically found in carbon materials derived from biomass pyrolysis. In particular, the band observed at approximately 1747 cm^{-1} can be attributed to C═O stretching vibrations from carbonyl or carboxyl groups, while the band around 1535 cm^{-1} is related to aromatic C═C skeletal vibrations [45,46]. Additional absorption bands located near 1060 cm^{-1} and 957 cm^{-1} can be assigned to C–O stretching vibrations from residual oxygenated functionalities such as phenols, alcohols, or ethers on the carbon surface [46]. The FT-IR spectrum of the PDMS sponge follows the characteristic absorption bands of polydimethylsiloxane [47]. The bands in the 1000–1100 cm^{-1} region correspond to Si–O–Si stretching vibrations, while the band near ~1260 cm^{-1} is attributed to Si–CH_3 deformation. In addition, the peak around ~2960 cm^{-1} corresponds to C–H stretching vibrations of methyl groups, and the band near ~800 cm^{-1} is assigned to Si–CH_3 rocking vibrations, confirming the PDMS chemical structure [24,48]. The spectrum of the Cork–PDMS composite mainly reproduces the characteristic bands of PDMS, indicating that the polymeric structure remains unchanged after the incorporation of carbon-based material. The spectral contribution of cork-related functional groups is relatively weak and partially masked by the dominant PDMS absorption bands. No significant peak shifts, new absorption bands or changes in peak intensity ratio are observed compared with the pristine PDMS spectrum. These results indicate that the addition of cork does not induce the formation of new chemical bonds with the PDMS matrix. Therefore, the composite formation is mostly governed by physical incorporation of pCork within the PDMS network rather than covalent chemical bonding.

Thermogravimetric (TGA) residue analysis was used to estimate the effective carbon content in the final composites (Fig. 2c and Figure S5). Since PDMS itself leaves a residual mass at high temperature, the amount of cork-derived carbon was determined by calculating the difference between the residual mass of neat PDMS and that of the pCork–PDMS composites at 600 °C under nitrogen atmosphere, where the curves reach a stable plateau. Based on this analysis, the resulting cork-to-PDMS mass ratios in the final composites were approximately ~5%, 10%, and 15% for the three formulations, in good agreement with the initial filler loadings used during fabrication. These values follow the same increasing trend as the initial pCork loadings used during fabrication, confirming that increasing the initial filler content results in higher incorporation of cork-derived carbon within the composite.

The incorporation of cork-derived carbon notably influenced the surface and interfacial properties of the final material. At lower amount of cork in the composite (5% with respect the total mass of the material) the sponge exhibited an improved hydrophobicity (140.3 ± 4.7 °) compared to a sponge composed of only PDMS (WCA = 131.4 ± 6.5 °). Increasing the amount of cork at 10 or 15%, WCA increases to 151.7 ± 2.7 and 151.2 ± 3.7 ° respectively (Fig. 2d). Therefore, the sponges exhibited superhydrophobic behaviour, with WCA exceeding 150°, a threshold reached as soon as 5 wt% of pCork was incorporated. Beyond this concentration, further increases in pCork content did not provide any significant enhancement in hydrophobicity, suggesting that higher loadings offer no additional advantage in terms of water repellency. In particular, it can be seen from (Fig. 2e and Video S1) that water adhesive forces are low on composites prepared with at least 5% of cork due to surface superhydrophobicity, and a water droplet can be easily pulled away from the PDMS-pCork sponges without any residue. The observed superhydrophobicity (WCA >150°) arises from the low surface energy of PDMS combined with hierarchical roughness. This roughness is generated by the NaCl-templated macroporous structure and the presence of cork-derived carbon particles. Increasing the pCork loading further enhances the surface roughness and the fraction of hydrophobic carbon domains exposed at the surface, which contributes to the progressive increase in WCA observed for the composite formulations. This multiscale roughness promotes a Cassie–Baxter regime, where trapped air pockets reduce the solid–liquid contact area. Moreover, all materials showed superoleophilicity, as demonstrated by the instantaneous sorption (less than 50 ms) of oil droplets with contact angles approaching 0°. During the sorption process, the sponge swells, a characteristic that is particularly useful, as it enables the material to efficiently accommodate and retain large quantities of oil (Fig. 2f and Video S2,3). It should be noted that, due to the macroporous architecture generated by the NaCl hard-templating process, the external surface of the sponge is not perfectly planar. As a result, slight local tilting of the surface may be observed during contact angle measurements. However, the wettability measurements were performed on multiple independently prepared samples, yielding highly reproducible values with small standard deviations, confirming the robustness of the superhydrophobic behaviour.

Supplementary material related to this article can be found online at doi:10.1016/j.jhazmat.2026.142088.

The intrinsic mechanical robustness of the porous scaffold was assessed by cyclic compression tests up to 60% strain. The pCork–PDMS sponge containing 5% of cork exhibited a compressive stress of 0.19 MPa at 60% strain, which is approximately one order of magnitude higher than that of pristine PDMS with comparable porosity, clearly evidencing the reinforcing effect of the pyrolyzed cork filler. This enhancement can be ascribed to the formation of a mechanically percolating carbonaceous network within the elastomeric matrix, which increases load transfer efficiency and limits pore wall collapse under large deformations. Furthermore, the composite showed a loss of compressive strength below 5% after 100 loading–unloading cycles at 60% strain, indicating high fatigue resistance and structural integrity. This mechanical stability further supports the formation of a well-interconnected macroporous network and effective NaCl removal. In templated sponge systems, incomplete template removal caused by poorly connected pores typically leads to residual crystals and structural weakness under repeated mechanical deformation. Such strong

durability under repeated compression–release operations is particularly relevant for oil–water separation applications, where multiple squeezing cycles are required for sorbent regeneration, and underscores the key role of the pCork filler in imparting both stiffness and long-term mechanical stability to the porous PDMS framework (Fig. 2i,j).

Qualitative electrical measurements using a digital multimeter confirmed a modest increase in electrical conductivity, further supporting the uniform distribution of the conductive filler throughout the sponge structure (Figure S6). The presence of the carbon phase also imparted a darker colour, a desirable feature in oil-adsorbent materials for both tracking and operational handling.

Overall, the combined use of pyrolysis, mechanochemical processing, salt templating, and microwave-assisted polymerization enabled the fabrication of composite sponges that are structurally robust, chemically stable, and functionally advanced. The cork-derived pyrolyzed filler not only contributed to microwave absorption and curing efficiency but also enhanced surface wettability and structural integrity. Moreover, this green, scalable, and controllable strategy lays the foundation for the reproducible fabrication of high-performance composite sponges from upcycled biomass sources.

3.3. Oil sorption properties of pCork-PDMS sponges

The oil sorption performance of pCork-PDMS sponges was systematically investigated by testing composites with different amounts of incorporated cork-derived carbon. As stated above, three formulations were prepared, containing 5, 10, and 15 wt% pCork relative to the mass of the sponge. Interestingly, the sponge prepared using 10 wt% pCork with respect the template exhibited the highest oil sorption capacity for ethyl acetate with an absorbance value of M_{Abs}= 7.51 g g^{-1}, i.e. about 10% higher than the other samples (Fig. 3a). This non-linear trend can be rationalized considering that a moderate amount of carbon filler optimizes both the porosity and the swelling behaviour of the composite: at low filler content (5 wt%), the available surface area and hydrophobic domains may be insufficient to maximize oil uptake, while at higher loading (15%), excessive carbon can lead to partial pore blockage or reduced flexibility of the PDMS matrix, limiting the overall sorption efficiency. To further clarify the role of the carbon filler in the composite structure, BET surface area measurements were performed on pristine PDMS and on the pCork–PDMS sponge containing 5 wt% carbon (Figure S7). It should be noted that BET analysis is primarily sensitive to micro- and mesoporous structures and therefore provides limited information for materials dominated by large macropores such as templated polymeric sponges. Consistently, only a slight increase in specific surface area was observed for the pCork–PDMS (S_{BET} = 0.232 ± 0.004 m^2/g) composite compared to pristine PDMS (S_{BET} = 0.075 ± 0.004 m^2/g). This modest increase likely reflects the presence of microporous features associated with the cork-derived carbon particles.

However, the limited variation in BET surface area indicates that the enhanced sorption performance observed for the composite cannot be primarily attributed to surface area effects. Instead, oil uptake is predominantly governed by the macroporous architecture generated by the NaCl templating process together with the swelling capability of the elastomeric PDMS matrix, which together provide a substantially larger solvent-accessible volume than that captured by BET measurements.

For all the other characterization pCork-PDMS sponge with 10% in weight of carbonaceous material have been used

To further elucidate the sorption dynamics, the kinetics of oil uptake were evaluated using ethyl acetate as a model solvent. Interestingly, the pCork-PDMS sponge achieved more than 95% of its sorption capacity within just 30 s (Fig. 3b). This rapid uptake reflects the high permeability and interconnected porosity of the material. It also indicates strong affinity between the sponge surface and the organic phase. Moreover, the sponge's ability to swell during sorption (Fig. 3d, S8 and video S3) further enhances its capacity by accommodating larger volumes of oil within its porous network, making it highly effective for

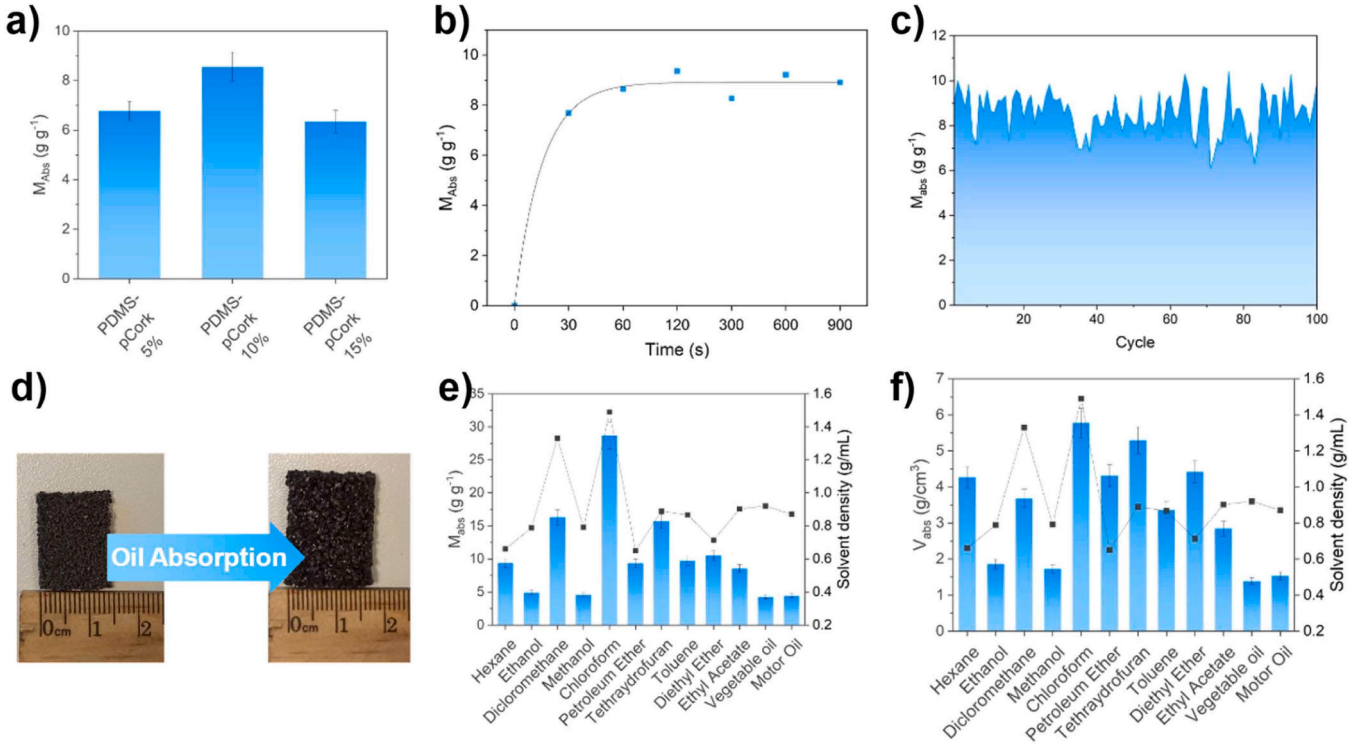

Fig. 3. sorption performance and recyclability of pCork-PDMS sponges. (a) Mass sorption capacity for composite sponges with varying pCork loadings (5%, 10%, 15% wt.). (b) Kinetics of oil uptake over time by pCork-PDMS sponge. (c) Cyclic oil sorption and desorption tests over 100 cycles. (d) Photographs illustrating sponge swelling after oil sorption. (e) Mass sorption capacities of pCork-PDMS sponge for different organic solvents. (f) Corresponding volume sorption capacities for different organic solvents.

rapid and substantial oil uptake.

The reusability and mechanical stability of the sponges were assessed through repeated sorption–desorption cycles using oil. The sponge maintains stable sorption capacity over 100 sorption–desorption cycles, with no statistically significant decline in performance (Fig. 3c). In addition, no measurable mass loss was detected after repeated cycling further confirming structural integrity and resistance to pore collapse. This exceptional durability is attributed to the robust crosslinked PDMS network and the stable integration of the cork-derived carbon filler, which together prevent material fatigue and degradation even under intensive operational conditions. Notably, the strong resistance observed under repeated sorption cycles is consistent with the mechanical testing results presented in Fig. 2i,j, where the composite exhibited high compressive strength and good fatigue resistance, confirming the mechanical reinforcement imparted by the cork-derived carbon network and its critical role in long-term operational durability. Unlike purely biomass-derived aerogels that rely on weakly crosslinked or hydrogen-bonded networks and may undergo irreversible pore collapse under wet conditions, the present composite benefits from a crosslinked elastomeric PDMS matrix. This elastomeric framework ensures full macroscopic recovery after repeated compression (60% strain, 100 cycles) and prevents structural degradation during oil sorption. No permanent deformation or pore collapse was observed throughout testing.

Oil sorption tests conducted with various organic solvents revealed mass sorption capacities ranging from 4.9 to 28.7 g g^{-1} , depending on the density, viscosity, and surface tension of the tested liquids (Fig. 3e). To provide a more application-relevant assessment, we calculated the volume sorption capacity for different solvents (Fig. 3f). Direct comparison based solely on gravimetric sorption capacity (g g^{-1}) can be misleading, as this metric is strongly influenced by bulk density. Ultralight aerogels often report very high g g^{-1} values primarily due to their extremely low density rather than intrinsically superior oil uptake efficiency. By contrast, volumetric sorption capacity directly reflects the actual volume of oil that can be removed per unit volume of absorbent, making it more representative of practical deployment conditions. When expressed on a volumetric basis, the sorption performance of the pCork–PDMS sponge falls within the range reported for several PDMS/carbon composites [8,12,24,48–61] and higher than many traditional carbon aerogels [17,62–64] and compares favorably with many lightweight porous sorbents reported in the literature [18,20,64]. When normalized by density, the apparent performance gap between ultralight aerogels and mechanically robust composites is significantly reduced (Table S1). The present system therefore achieves a favorable balance between volumetric sorption performance and mechanical resilience, maintaining structural stability over repeated cycling. These results highlight the practical robustness and versatility of the material across a range of oil types and operational scenarios.

The superior sorption behavior can be attributed to the pronounced swelling properties of the composite. Much like hydrogels which are able to absorb and retain large amounts of water due to their flexible, three-dimensional polymeric network, the pCork-PDMS sponge exhibits a similar mechanism in the presence of oils. Upon contact with oil, the material swells significantly, increasing its internal volume enhancing its overall sorption capacity (Figure S8 and Video S3). This oilgel-like behavior results from the synergistic combination of the open-cell porous architecture and the intrinsic affinity of the PDMS matrix and cork-derived carbon for organic liquids, which enables the efficient uptake and retention of various oils.

In summary, the variation in sorption capacity arises from multiple physicochemical factors, including solvent density, polarity, and interaction with the PDMS–pCork framework. First, the gravimetric sorption capacity (g g^{-1}) is partially influenced by solvent density. Denser liquids, such as chloroform and dichloromethane, naturally produce higher mass uptake values because a larger mass of solvent can occupy the same pore volume. However, the volumetric sorption capacity follows a similar trend, indicating that density alone does not fully account for the observed differences. Second, solvent polarity and compatibility with the composite surface play an important role. The PDMS matrix and the graphitic carbon domains derived from pCork provide a predominantly hydrophobic and organophilic surface. Consequently, polar protic solvents such as methanol and ethanol show limited affinity for the composite and therefore exhibit lower sorption capacities, whereas nonpolar or weakly polar organic solvents interact more favorably with the PDMS–carbon network. Finally, several solvents tested in this study (e.g., chloroform, THF, and toluene) are known to induce swelling of PDMS, which facilitates solvent penetration into the elastomeric matrix and enhances uptake within the macroporous structure.

Porosity of the composite was also evaluated using the density-based approach described in the Eq. (1), the structural porosity of the pCork–PDMS sponges was estimated from the measured bulk density of the material (0.30 g cm^{-3}) and the density of the dense PDMS phase (≈0.97 g cm^{-3}). This yields a structural porosity of approximately 69%, confirming the highly porous architecture generated by the NaCl hard-templating strategy. Interestingly, when solvent uptake measurements are converted into an apparent porosity (Eq. 2) using methanol as probing liquid, the calculated apparent porosity exceeds 100%. This value does not represent a true structural porosity; rather, it reflects the combined contribution of pore filling and solvent-induced swelling of the PDMS matrix during sorption. Instead, methanol sorption involves a combination of macropore filling and solvent-induced swelling of the PDMS matrix, which increases the accessible free volume during sorption. Consequently, the overall sorption capacity of the composite cannot be interpreted solely on the basis of static structural porosity. This swelling-assisted uptake mechanism contributes to the high sorption performance observed for the composite. While ultralight aerogels often exhibit higher intrinsic porosity, their uptake capacity is largely determined by the fixed pore volume of the structure and they frequently suffer from limited mechanical robustness. In contrast, the elastomeric nature of PDMS enables reversible swelling upon contact with organic liquids, effectively increasing the accessible storage volume beyond the initial pore network. The ability of the pCork–PDMS sponge to maintain stable sorption performance over more than 100 absorption–desorption cycles (Fig. 3c) further indicates that this swelling behavior is reversible and does not lead to structural collapse of the porous framework. From a practical standpoint, this behavior may also offer operational advantages. The material can be transported in its compact dry state, while additional solvent-accessible volume develops only upon contact with oil or organic solvents. As a result, the effective sorption capacity during operation can exceed the value predicted from the static pore structure alone. Altogether, the combination of templated macroporosity and reversible polymer swelling provides a dual mechanism for liquid uptake, contributing to the high sorption efficiency and mechanical durability of the pCork–PDMS composite. The combined influence of density, solvent polarity, and swelling-induced affinity with the PDMS–pCork framework therefore explains the systematic variation observed in the sorption capacities of the different organic solvents.

Overall, these findings demonstrate that the pCork-PDMS sponge is a highly effective, robust, and reusable oil sorbent, with rapid uptake kinetics and superior sorption capacities compared to many conventional and advanced materials reported in the literature. The synergy between the sustainable fabrication strategy and the advanced functional properties of the material underscores its potential for large-scale oil spill remediation and industrial wastewater treatment.

3.4. Biocompatibility of pCork-PDMS sponges

Biological safety is an often overlooked aspect in the development of sorbent materials for environmental remediation. While most oil–water separation studies focus primarily on removal efficiency and sorption capacity, the potential biological impact of the remediation material itself is rarely considered. However, during oil spill response or

wastewater treatment, sorbent materials are frequently deployed directly in natural environments where they may interact with aquatic organisms, release small fragments, or generate leachates that may enter surrounding ecosystems. Assessing the biological response to these materials therefore represents an important step toward the development of safer-by-design remediation technologies.

In this context, the present study evaluates the biological response to the pCork–PDMS sponges under realistic exposure scenarios, considering both direct contact with the material surface and indirect exposure through aqueous media previously in contact with the material. These exposure routes were selected to assess potential biological interactions during material handling and environmental contact.

Two complementary cell models were used to probe different potential exposure routes. Human keratinocyte cells (HaCaT) were employed as a representative model for dermal contact exposure, which may occur during material handling or environmental deployment. In parallel, oral epithelial carcinoma cells (OECM-1) were used to evaluate potential responses associated with ingestion-related or mucosal exposure pathways. To reproduce these exposure conditions, two experimental approaches were implemented. In the direct exposure experiments, cells were cultured in contact with the sponge surface to assess potential cytotoxic responses arising from the material itself. In the indirect exposure experiments, cells were exposed to conditioned aqueous media previously incubated with the sponges, allowing the evaluation of possible biological effects associated with soluble components or released species. Together, these complementary assays provide a preliminary evaluation of the biological safety of the material, providing preliminary information on its biological response profile and supporting the responsible deployment of biomass-derived sorbent materials for oil–water remediation. Indirect cytotoxicity was evaluated by incubating pCork-PDMS and PDMS sponges in culture medium for 24 h, after which the conditioned medium was used to culture HaCaT and OECM-1 cells at concentrations of 100 μg ml^{-1} and 1 mg ml^{-1}. The MTT assay results (Fig. 4b-d) demonstrated good cell viability, with OECM-1 cells maintaining over 90% viability and HaCaT cells exhibiting nearly 100% viability after 24 h of exposure for both the materials, indicating the absence of toxic leachable compounds.

To further probe direct interactions, cells were seeded onto the sponge surfaces to evaluate adhesion, morphology, and proliferation. Confocal microscopy revealed that stained nuclei maintained typical morphology without signs of chromatin condensation or apoptotic features. These findings confirm that both pCork-PDMS composite sponges support cell viability and proliferation without eliciting cytotoxic responses. Collectively, these data establish that the pCork-PDMS sponges exhibit a high degree of biocompatibility across multiple, biologically relevant exposure routes. This comprehensive evaluation not only supports the safe environmental deployment of these materials but also informs potential occupational health considerations for handlers and end-users.

3.5. Application of pCork-PDMS sponges in water oil separation

The oil–water separation performance of the pCork-PDMS sponge as passive system was systematically evaluated using both surface and submerged oil models, in order to simulate diverse real-world spill scenarios and to assess the versatility and the selectivity of the material under challenging conditions. Ethyl acetate was selected as a representative surface oil, while chloroform was chosen to model submerged oil contaminants; both were stained with green liposoluble dye to facilitate visual monitoring. Upon introduction of the pCork-PDMS sponge to the oil–water mixtures, the material rapidly and selectively removed the oil phase, regardless of whether it was floating on the surface or located beneath the water (Fig. 5a,b and Video S4,5). In the case of ethyl acetate, the sponge selectively removed the oil layer from the water surface, leaving the aqueous phase visibly clear and free of any residual coloration. When used to capture submerged chloroform, the sponge efficiently absorbed the oil upon gentle immersion below the water surface, resulting in a transparent aqueous phase.

Supplementary material related to this article can be found online at doi:10.1016/j.jhazmat.2026.142088.

Interestingly, during the sorption of submerged oils, the pronounced superhydrophobicity of the pCork-PDMS sponge leads to the formation

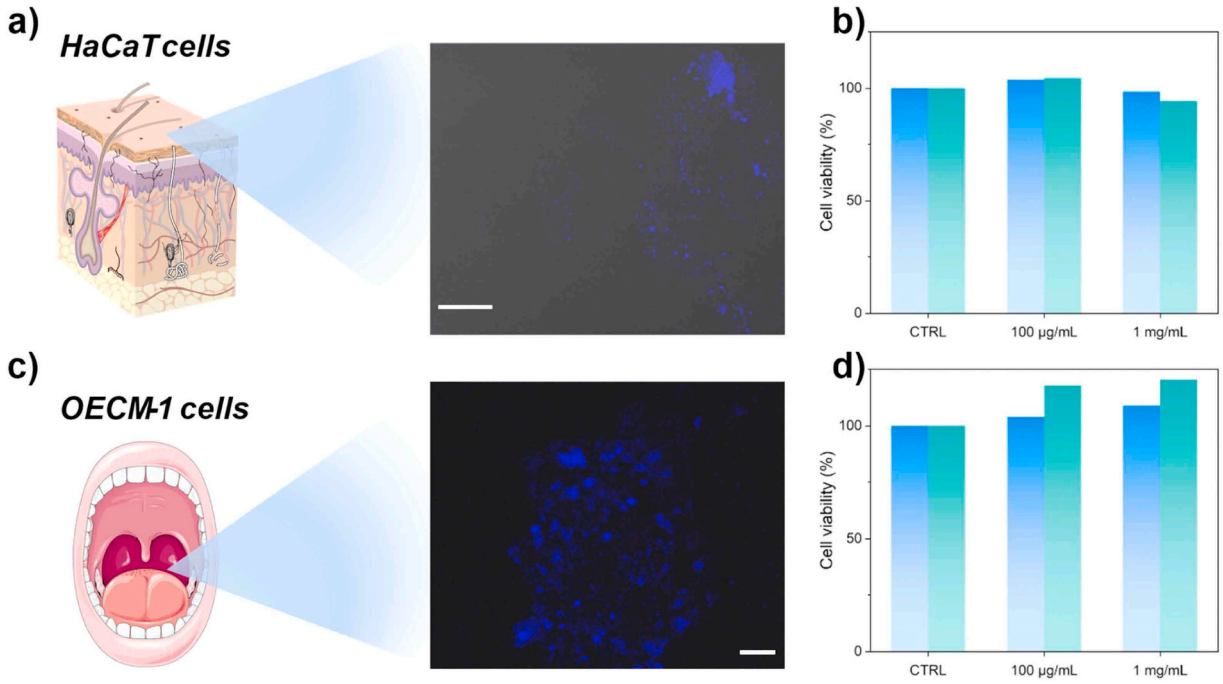

Fig. 4. (a, c) Representative confocal microscopy images of HaCaT (a) and OECM-1 (c) cells cultured on sponge surfaces after 24 h; DAPI-stained nuclei in blue, scale bar = 100 μm. (b, d) Cell viability assessed by MTT assay for HaCaT (b) and OECM-1 (d) cells after exposure to conditioned medium with different sponge concentrations; blue bars correspond to pCork-PDMS sponges, green bars to PDMS-only sponges.

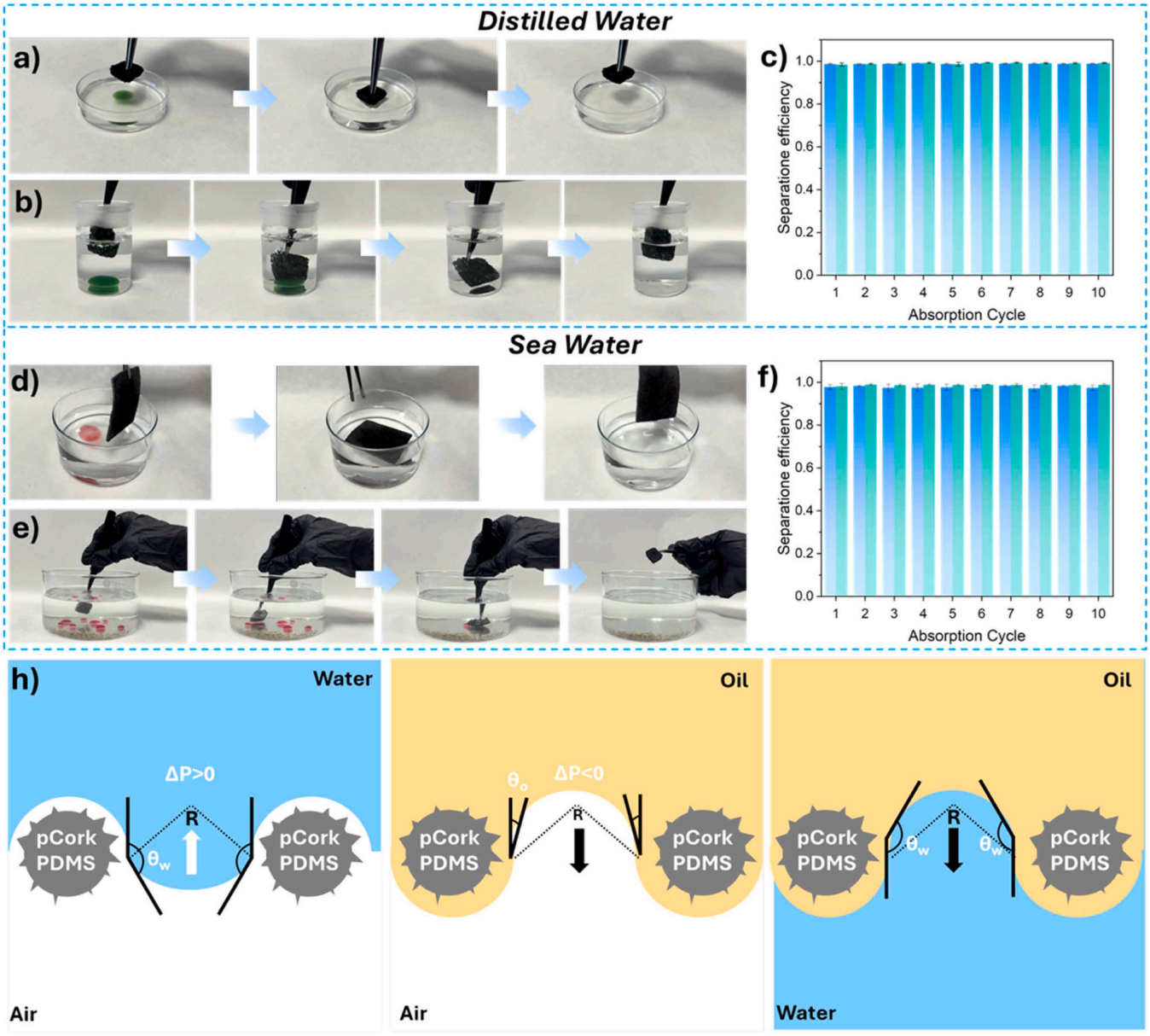

Fig. 5. (a–b) Sequential images demonstrating the separation of surface oil (a) and submerged oil (b) from distilled water using the sponge. (c) Histogram of separation efficiency over multiple sorption cycles in distilled water; blue bars correspond to surface oil removal, while green bars indicate submerged oil removal. (d–e) Sequential images showing the removal of surface (d) and submerged (e) oil from real seawater. (f) Separation efficiency in real seawater over ten cycles, again distinguishing between surface (blue) and submerged (green) oil. (h) Schematic illustration of the oil–water separation mechanism based on the Young–Laplace equation: left, selective water exclusion; center, oil penetration in air; right, oil entry in a water environment, highlighting the interplay of pressure and wettability.

of a persistent air layer around the material when immersed in water. This air cushion effectively prevents water from penetrating the porous structure, thereby facilitating selective oil uptake. This phenomenon is characteristic of superhydrophobic surfaces and was directly observed during the experiments. As the sponge began to absorb the chloroform phase, the displacement of the air layer was evidenced by the release of air bubbles from the material (Fig. 5b and Video S5). This observation confirms that the interior of the sponge remains unwetted by water, and that oil sorption occurs through the replacement of the air cushion with the organic phase. The presence and persistence of this air layer, together with the visible escape of bubbles during oil uptake, provide clear evidence of the material's ability to exclude water and maintain selective sorption even under submerged conditions.

The oil removal efficiency was conclusively demonstrated to be on average ~99% for both surface and submerged oils in distilled water, as shown in Fig. 5c. The high separation efficiency indicates that only a negligible fraction of oil remains in the aqueous phase after treatment. This consistently high performance over multiple sorption cycles confirms the sponge's good selectivity and capacity to effectively separate oils from water, establishing its reliability for practical oil–water separation applications. Overall, these results indicate that the pCork-PDMS sponge achieves removal of both surface and submerged oils from water, with a level of selectivity and efficiency at least comparable to, and in some respects superior to, advanced nanocarbon-based PDMS composites [8,12,24,48–61].

The oil–water separation performance of the pCork-PDMS sponge was also assessed using real seawater samples to better simulate operational conditions; This test is important to assess the usability of these composites in real marine environments. Complex factors such as high ionic strength, presence of organic matter, suspended solids, and varying pH can affect sorbent behavior and durability. Unlike many studies that rely solely on pure lab-grade solutions, this work utilized real seawater

samples directly collected from the marine environment, providing a more realistic evaluation of the sponge's robustness and functional stability. In this case, the oil was stained with Oil Red O. The material was able to remove both suspended and submerged oils (Fig. 5d,e and Video S6,7) maintaining high separation efficiency (Fig. 5 f) in real seawater. The good performance shown by these larger samples confirms the scalability of the fabrication process. In addition to real seawater, the chemical robustness of the sponge was also evaluated in strongly acidic (1 M HCl, Video S8) and basic (1 M NaOH) (video S9) environments, where the material maintained efficient oil–water separation performance (Figure S9a,b). These experiments demonstrated that despite the chemically and physically harsh conditions, the pCork-PDMS sponge preserved rapid and selective oil uptake, affirming its applicability beyond idealized laboratory settings. Interestingly also hydrophobicity is preserved once the material is in contact with harsh solutions (figure S9c). Moreover, the sponge was able to efficiently remove motor oil from water (Figure S9d and Video S10) with negligible increment in sponge weight after different adsorption-desorption cycles, thus suggesting the absence of significative fouling phenomena (Figure S9e). The material was also able to capture oil droplets from surfactant-stabilized oil-in-water emulsions (Figure S10) simply by contacting the material with the stirred emulsion, without the need for external pressure or filtration systems.

Supplementary material related to this article can be found online at doi:10.1016/j.jhazmat.2026.142088.

The combination of superhydrophobicity, superoleophilicity, and robust mechanical properties ensures that water is effectively excluded from the sponge structure during operation in a passive way without the help of external forces, facilitating a straightforward oil recovery and a repeated reuse of the material. The robust performance observed even in real seawater matrices further highlights the practical relevance of this material for real-world oil spill remediation and wastewater treatment, confirming that the sustainable design and fabrication strategy translates directly into strong functional performance in oil–water separation.

The high selectivity and efficiency of the pCork–PDMS composite can be explained by the interplay between pore structure, interfacial properties, and capillary phenomena, as described by the Young–Laplace equation:

$$\Delta P = \frac{2\gamma\cos\theta}{r}$$

where γ is the liquid–air interfacial tension, θ is the contact angle of the liquid on the pore wall, and r is the effective pore radius. The measured WCA of 151.7° classifies the material as superhydrophobic, while the contact angle for both ethyl acetate (used as floating oil) and chloroform (used as submerged oil) was found to be 0°, indicating superoleophilicity. SEM analysis revealed an average macropore diameter of 407.3 ± 59.2 μm (Figure S3a-c), consistent with the NaCl template size distribution (Figure S3d). This macroporous architecture facilitates capillary-driven oil sorption while preserving interconnected pathways for fluid transport. Using the Young–Laplace relation, the calculated capillary pressure for water is $\Delta P \approx -620$ Pa ($\theta = 151.7°$, $r = 2.04 \times 10^{-4}$ m). The negative sign indicates resistance to spontaneous water infiltration. The magnitude of this value corresponds to a hydrostatic head of approximately 6 cm. This means that an external pressure exceeding this threshold would be required to force water penetration into the pores. Accordingly, when immersed, the sponge maintains a stable air layer within its pore network, as evidenced by the release of air bubbles upon contact with a submerged oil phase (Fig. 5 h).

Conversely, the extremely low contact angle of both oils, paired with their respective interfacial tensions (23.9 mN/m for ethyl acetate and 27.1 mN/m for chloroform), establishes a highly favorable capillary pressure for oil imbibition ($\Delta P \approx 234$ Pa and ≈265 Pa respectively), driving rapid oil uptake.

These values were estimated assuming liquid imbibition into air-filled pores ($\gamma_{liquid/air}$), consistent with the experimentally observed persistence of the interfacial air layer during submerged oil contact. Under these conditions, phase selectivity is governed by the sign of the capillary pressure: water generates a negative capillary pressure, resisting spontaneous infiltration, whereas oils, owing to their near-zero contact angle, produce a positive capillary driving force that actively promotes imbibition

It is important to emphasize that macroporous sorbent sponges of this type are not intended to function as hydrostatic pressure barriers or deep-water filtration membranes. Rather, separation is dictated by interfacial energetics and selective wettability. Oil uptake occurs through preferential infiltration into oleophilic pore walls, locally displacing water at the oil–solid interface without requiring sustained hydrostatic exclusion. Furthermore, local pore constrictions smaller than the average macropore diameter would increase the effective capillary pressure, reinforcing oil-selective imbibition.

Altogether, the combination of large interconnected pores, superoleophilicity (zero contact angle for oil), and superhydrophobicity (WCA >150°) creates an optimized capillary environment for efficient oil capture and water exclusion. The ability to quantitatively rationalize separation performance through the Young–Laplace framework validates the material design and supports its application as a green alternative for oil–water remediation compared to conventional polymeric and carbonaceous sorbents.

In Table 1 the performance of the pCork–PDMS sponge is benchmarked against previously reported PDMS/carbon composite sorbents. Its gravimetric sorption capacity is comparable to state-of-the-art systems, with variations largely attributable to differences in solvent properties, pore architecture, and material density. Rather than maximizing a single performance metric, the present composite is designed to integrate high separation efficiency, superhydrophobicity (WCA >150°), rapid capillary-driven oil uptake, and stable reusability over extended cycling.

In addition, the pCork–PDMS sponge represents one of the few PDMS–carbon systems for which biocompatibility has been experimentally assessed, further supporting its environmental compatibility. Taken together, the metrics summarized in Table 1 highlight a balanced combination of durability, recyclability, structural robustness, and efficient oil sorption, addressing several practical limitations associated with conventional porous sorbents.

Moreover, beyond separation performance, lifecycle considerations are also important when evaluating sorbent materials intended for environmental remediation. From a lifecycle perspective, the pCork–PDMS sponge is designed to be mechanically regenerated through repeated sorption–squeezing cycles, enabling recovery of absorbed oil and extended reuse of the material. At the end of its operational lifetime, disposal options may include controlled incineration or thermal treatment, allowing energy recovery while minimizing environmental release. Compared with sorbents based on engineered nanocarbons such as carbon nanotubes or graphene nanoplatelets, the present composite may present reduced ecotoxicological concerns because the carbon phase is derived from biomass pyrolysis and remains embedded within a stable polymeric matrix, limiting the potential release of free nanostructures into the environment.

Despite the here presented material has been intended as passive separation system, the mechanical robustness and rapid capillary-driven oil sorption of the pCork–PDMS sponges also suggest potential integration into scalable oil–water separation systems, such as modular sorbent units, floating remediation platforms, or continuous separation devices. Similar porous sorbent architectures have recently been proposed for larger-scale environmental remediation systems, highlighting the feasibility of translating laboratory-scale sorbent materials into practical separation technologies [65,66].

Table 1
Comparative performance benchmarking of pCork-PDMS sponges and representative PDMS/carbon-based sorbents for oil–water separation. The table reports the values for WCA, reusability over multiple sorption cycles, mass sorption capacity (Mabs) ranges, sorption time to reach more than 90% of the sorption capacity, and biocompatibility for various materials.

Material	Mass Sorption capacity ranges (G G^{-1})	WCA (°)	Reusability (n° Cycles)	sorption time (s)	Biocompatibility
This work	28.7–4.9	151.7	> 100	30	Yes
PDMS-NH_2/ CCNTs [49]	27–10	144.3	30	80	n.a.
mMWCNTs/ PDMS [12]	20.5–8.8	153.4	50	120	n.a.
PDMS/CNTs [50]	33–14	121.8	5	30	n.a.
PDA/CNTs/ PDMS [51]	15–5	137.9	n.a.	60	n.a.
PDMS/ PDMAEMA [52]	11.5–5	140	n.a.	n.a.	n.a.
PDMS/ Graphene [53]	17–5	151	10	n.a.	n.a
PDMS/GO [54]	15–4	147.1	10	300	n.a.
PDMS-NH_2/ GO [48]	17–5	138.1	30	50	n.a.
rGO/PDMS/ PEI [24]	16–3	130	60	300	n.a.
rGO/GCC/ PDMS [55]	25–10	152	10	1800	n.a.
PDMS-Gr [56]	14–4	130.8	15	n.a.	n.a.
F-GR/PDMS [57]	12–5	150	20	n.a.	n.a.
PDMS-gR aerogel [58]	11–4	152.7	10	n.a.	n.a.
PDMS/CuS/ CFs/RGO [8]	25–13	138.4	10	n.a.	n.a.
PDMS-CNF [59]	11.5–5	153	10	n.a.	n.a.
PDMS-CNF [60]	8.5–1.5	150	10	n.a.	n.a.
CB/PDMS [61]	26–3	125	10	15	n.a.

4. Conclusion

This work reports a sustainable strategy for fabricating porous PDMS sponges that incorporate graphitic carbon derived from cork industrial waste through mechanochemical processing and microwave-assisted polymerization. The resulting pCork-PDMS composites address key limitations of earlier oil-absorbing systems, including surface fouling, slow uptake rates, and challenges related to energy efficiency, scalability, and biocompatibility.

By utilizing pyrolyzed cork as a scalable, low-impact alternative to traditional nanocarbons, this approach avoids hazardous reagents and energy-intensive steps and supports a circular economy by valorizing industrial byproducts. Mechanochemical activation ensures fine particulate dispersion through non-covalent interactions and enhanced compatibility between the carbon phase and polymer matrix, yielding monolithic sponges with interconnected porosity and pronounced superhydrophobic–superoleophilic properties. This combination results in materials that are robust, readily regenerated, and capable of rapid and efficient oil–water separation, including for submerged contaminants and in real seawater matrices.

In contrast to many PDMS/carbon-based sorbents reported in the literature, which typically optimize only one or two performance metrics at the expense of others, the pCork-PDMS platform achieves a concurrent and balanced combination of key functional properties, including superhydrophobicity, rapid uptake kinetics, high mass sorption capacity, mechanical durability over repeated regeneration cycles, and good separation efficiency for both floating and submerged oils.

This integrated performance profile supports the use of mechanochemically processed cork-derived carbon as a viable alternative to synthetic nanocarbons in PDMS-based sorbents. In contrast to many studies that overlook the bio-environmental impact of sorbents, we provide a thorough assessment of biocompatibility through both indirect (leachate) and direct (surface contact) exposure on representative human cell models, showing no detectable acute cytotoxic effects under the tested conditions and supporting a preliminary safety profile for environmental deployment in sensitive environmental and occupational settings.

Because the carbon phase is biomass-derived and embedded within a stable PDMS matrix, the material may present a lower risk of releasing free carbon nanostructures than sorbents based on engineered nanocarbons.

Overall, these findings advance the field of passive oil–water separation by combining green materials chemistry with practical remediation technologies. Beyond separation efficiency and materials sustainability, this work highlights the importance of integrating safety-by-design principles into the development of sorbents for hazardous liquid remediation. This approach establishes a transferable framework in which circular feedstocks, solvent-free processing, and demonstrated environmental safety are treated as co-requirements alongside separation performance, supporting the translation of laboratory-scale sorbents into operational tools for real-world oil spill response and industrial wastewater management.

Environmental implication

Oil spill pollution and industrial oily wastewater pose persistent threats to aquatic ecosystems. While passive, capillarity-driven separation technologies offer sustainable and rapid remediation, the environmental safety of sorbent materials themselves is often overlooked. Here, biocompatible and recyclable pCork–PDMS sponges are developed through the valorization of cork waste using a solvent-free mechanochemical route, reducing the lifecycle environmental footprint. The materials achieve > 95% oil removal within 30 s, retain performance over more than 100 cycles in real seawater, and exhibit no detectable cytotoxic effects, supporting their potential as a scalable and circular platform for sustainable marine and industrial water remediation.

CRediT authorship contribution statement

Antonio Turco: Writing – review & editing, Writing – original draft, Visualization, Validation, Supervision, Resources, Methodology, Investigation, Funding acquisition, Formal analysis, Data curation, Conceptualization. **Francesco Ferrara:** Writing – review & editing, Visualization, Validation, Supervision, Resources, Project administration, Funding acquisition. **Antonio Grieco:** Visualization, Supervision, Funding acquisition. **Maria Serena Chiriacò:** Writing – review & editing, Writing – original draft, Visualization, Validation, Supervision, Methodology, Investigation, Conceptualization. **Clara Piccirillo:** Writing – review & editing, Writing – original draft, Visualization, Validation, Methodology, Investigation, Formal analysis, Data curation, Conceptualization. **Antonella Iaia:** Writing – original draft, Visualization, Validation, Methodology, Investigation, Formal analysis, Data curation, Conceptualization. **Roberta Di Maio:** Writing – original draft, Visualization, Validation, Methodology, Investigation, Formal analysis, Data curation. **Viviana Vergaro:** Writing – review & editing, Visualization, Validation, Supervision, Formal analysis. **Elisabetta Primiceri:** Writing – review & editing, Visualization, Validation, Supervision,

Methodology. **Valeria Garzarelli:** Writing – original draft, Visualization, Validation, Methodology, Investigation, Formal analysis. **Alessia Rinaldi:** Data curation, Formal analysis, Investigation, Methodology, Validation, Writing – original draft. **Concetta Nobile:** Writing – original draft, Visualization, Validation, Methodology, Investigation, Formal analysis, Data curation, Conceptualization.

Declaration of Generative AI and AI-assisted technologies in the writing process

During the preparation of this work the authors used Perplexity in order to check the language and improve the readability. After using this tool, the authors reviewed and edited the content as needed and take full responsibility for the content of the publication.

Declaration of Competing Interest

The authors declare that they have no known competing financial interests or personal relationships that could have appeared to influence the work reported in this paper.

Acknowledgements

We thank Dr. Elisabetta Perrone for her technical help in contact angle measurements and laboratory management.

This research was funded by Italian Ministry of Enterprises and Made in Italy: “MSP4WATER” Project funded within the frame of the Programme “Fondo per la Crescita Sostenibile—Accordi per l’innovazione DM 31/12/2021" (grant number: F/310200/01–04/X56); by Italian Ministry of University and Research (MUR), PRIN 2022 Project – financed by European Union – Next Generation EU - PNRR M4.C2.1.1. - MAGELLANO MAnufacturing systems for Graphene nanocompositEs and their appLications as embedded eLectrochemicAl seNsors in Lab-On-chip (grant number: 2022NRMS4X) CUP: B53D23008860006; PRIN 2022 PNRR Project – financed by European Union – Next Generation EU - PNRR M4.C2.1.1. - CALINERO Enhancing Neurovascular Communication with Carbon-engineered Organs-on-a-Chip: Novel Nanotools for Brain Injury Repair (CALINERO) (grant number: P2022TKL5T) CUP: B53D23028310001; by Regione Puglia within “Tecnopolo per la medicina di precisione” (TecnoMed Puglia): DGR n.2117 del 21/11/2018, CUP: B84I18000540002 and Italian Ministry of Research (MUR) under the complementary actions to the NRRP (PNC0000007) “Fit4MedRob- Fit for Medical Robotics” Grant (contract number CUP B53C22006960001).

Appendix A. Supporting information

Supplementary data associated with this article can be found in the online version at doi:10.1016/j.jhazmat.2026.142088.

Data availability

Data will be made available on request.

References

[1] Chu, Z., Feng, Y., Xu, T., Zhu, C., Li, K., Li, Y., et al., 2023. Magnetic, self–heating and superhydrophobic sponge for solar–driven high–viscosity oil–water separation. J Hazard Mater 445, 130553.

[2] Guan, Y., Qiao, D., Dong, L., Chen, X., Wang, Z., Li, Y., 2023. Efficient recovery of highly viscous crude oil spill by superhydrophobic ocean biomass-based aerogel assisted with solar energy. Chem Eng J 467, 143532.

[3] Zhang, Y., Hou, S., Song, H., Qin, G., Li, P., Zhang, K., et al., 2023. A green and facile one-step hydration method based on ZIF-8-PDA to prepare melamine composite sponges with excellent hydrophobicity for oil-water separation. J Hazard Mater 451, 131064.

[4] Luo, Q.-R., Zhong, Y.-H., Chung, L.-H., Jiang, Z., Lin, Q.-C., Xu, X.-K., et al., 2023. A hydrophobic–superoleophilic 2D Zr-based alkyne-rich metal–organic framework for oil/water separation and solar-assisted oil evaporation. J Mater Chem A 11 (41), 22223–22231.

[5] Turco, A., Primiceri, E., Frigione, M., Maruccio, G., Malitesta, C., 2017. An innovative, fast and facile soft-template approach for the fabrication of porous PDMS for oil–water separation. J Mater Chem A 5 (45), 23785–23793.

[6] Alhassan, H., Soon, Y.W., Usman, A., Yoong, V.N., 2024. Ultrahydrophobic melamine sponge via interfacial modification with reduced graphene oxide/titanium dioxide nanocomposite and polydimethylsiloxane for oily wastewater treatment. Water Sci Eng 17 (2), 139–149.

[7] Worajittiphon, P., Majan, P., Wangkawong, K., Somsunan, R., Jantrawut, P., Panraksa, P., et al., 2024. Inside-out templating: a strategy to decorate helical carbon nanotubes and 2D MoS2 on ethyl cellulose sponge for enhanced oil adsorption and oil/water separation. Int J Biol Macromol, 133119.

[8] Ma, J., Ma, S., Xue, J., Xu, M., Zhang, J., Li, J., et al., 2023. Synthesis of elastic hydrophobic biomass sponge for rapid solar-driven viscous crude-oil cleanup absorption, oil-water separation and organic pollutants treating. Sep Purif Technol 305, 122512. https://doi.org/10.1016/j.seppur.2022.122512.

[9] Wan, W., Yang, Z., Tan, T., Li, Y., Zhang, Z., Zhang, P., et al., 2023. Three-dimensional hydrophobic melamine@ methyl trichlorosilane/polydimethylsiloxane sponge for consecutive and long-term oil/water separation. Chem Eng J 476, 146824.

[10] Zhang, T., Xiao, C., Zhao, J., Liu, X., Ji, D., Zhang, H., 2021. One-step facile fabrication of PVDF/graphene composite nanofibrous membrane with enhanced oil affinity for highly efficient gravity-driven emulsified oil/water separation and selective oil absorption. Sep Purif Technol 254, 117576.

[11] Yang, Y., Ren, Z., Zhou, C., Lin, Y., Shi, L., Hou, L., 2023. Anisotropic superhydrophobic graphene aerogel with radial superelasticity and axial superstiffness for efficient on-demand oil–water separation. J Mater Chem A 11 (36), 19524–19535.

[12] Turco, A., Malitesta, C., Barillaro, G., Greco, A., Maffezzoli, A., Mazzotta, E., 2015. A magnetic and highly reusable macroporous superhydrophobic/superoleophilic PDMS/MWNT nanocomposite for oil sorption from water. J Mater Chem A 3 (34), 17685–17696. https://doi.org/10.1039/c5ta04353k.

[13] Turco, A., Foscarini, A., Piccirillo, C., Primiceri, E., Chiriacò, M.S., Ferrara, F., 2024. A promising solution for water remediation: PDMS-(Nano)carbon hybrid materials for oil removal (https://doi.org/https://doi.org/). Appl Mater Today 38, 102218. https://doi.org/10.1016/j.apmt.2024.102218.

[14] Ben Rejeb, Z., Abidli, A., Zaoui, A., Fashandi, M., Selka, A., Naguib, H.E., et al., 2024. One-pot synthesis of rationally-designed flexible, robust, and hydrophobic ambient-dried molecularly-bridged silica aerogels with efficient and versatile oil/water separation applications. Adv Compos Hybrid Mater 7 (6), 188. https://doi.org/10.1007/s42114-024-00969-5.

[15] Lu, J., Feng, Q., Wang, J., Li, J., Tan, S., Xu, Z., 2024. Efficient solar-driven crude oil cleanup via graphene/cellulose aerogel with radial and centrosymmetric design (https://doi.org/https://doi.org/). J Hazard Mater 477, 135418. https://doi.org/10.1016/j.jhazmat.2024.135418.

[16] Wang, J., Shi, Z., Fan, J., Ge, Y., Yin, J., Hu, G., 2012. Self-assembly of graphene into three-dimensional structures promoted by natural phenolic acids. J Mater Chem 22 (42), 22459–22466. https://doi.org/10.1039/C2JM35024F.

[17] Sun, H., Xu, Z., Gao, C., 2013. Multifunctional, ultra-flyweight, synergistically assembled carbon aerogels. Adv Mater 25 (18), 2554–2560. https://doi.org/10.1002/adma.201204576.

[18] Zhao, Y., Hu, C., Hu, Y., Cheng, H., Shi, G., Qu, L., 2012. A versatile, ultralight, nitrogen-doped graphene framework. Angew Chem Int Ed 51 (45), 11371–11375. https://doi.org/10.1002/anie.201206554.

[19] Li, J., Li, J., Meng, H., Xie, S., Zhang, B., Li, L., et al., 2014. Ultra-light, compressible and fire-resistant graphene aerogel as a highly efficient and recyclable absorbent for organic liquids. J Mater Chem A 2 (9), 2934–2941. https://doi.org/10.1039/C3TA14725H.

[20] Nguyen, D.D., Tai, N.-H., Lee, S.-B., Kuo, W.-S., 2012. Superhydrophobic and superoleophilic properties of graphene-based sponges fabricated using a facile dip coating method. Energy & Environ Sci 5 (7), 7908–7912. https://doi.org/10.1039/C2EE21848H.

[21] Yang, S., Chen, L., Mu, L., Ma, P.-C., 2014. Magnetic graphene foam for efficient adsorption of oil and organic solvents. J Colloid Interface Sci 430, 337–344. https://doi.org/10.1016/j.jcis.2014.05.062.

[22] Vlachopoulou, M.E., Petrou, P.S., Kakabakos, S.E., Tserepi, A., Beltsios, K., Gogolides, E., 2009. Effect of surface nanostructuring of PDMS on wetting properties, hydrophobic recovery and protein adsorption. Microelectron Eng 86 (4), 1321–1324. https://doi.org/10.1016/j.mee.2008.11.050.

[23] Zhang, W., Wang, J., Han, X., Li, L., Liu, E., Lu, C., 2021. Carbon nanotubes and polydopamine modified poly (dimethylsiloxane) sponges for efficient oil–water separation. Materials 14, 2431.

[24] Tong, H., Chen, H., Zhao, Y., Liu, M., Cheng, Y., Lu, J., et al., 2022. Robust PDMS-based porous sponge with enhanced recyclability for selective separation of oil-water mixture. Colloids Surf A Physicochem Eng Asp 648, 129228. https://doi.org/10.1016/j.colsurfa.2022.129228.

[25] Song, S., Yang, H., Su, C., Jiang, Z., Lu, Z., 2016. Ultrasonic-microwave assisted synthesis of stable reduced graphene oxide modified melamine foam with superhydrophobicity and high oil adsorption capacities. Chem Eng J 306, 504–511.

[26] Zhao, J., Chen, H., Ye, H., Zhang, B., Xu, L., 2019. Poly (dimethylsiloxane)/graphene oxide composite sponge: a robust and reusable adsorbent for efficient oil/water separation. Soft Matter 15 (45), 9224–9232.

[27] Luo, L., Zhang, Q., Lan, Y., Deng, J., Lin, Y., Du, G., et al., 2023. Facile one-step synthesis of cork-derived hierarchical porous carbons with P, N, and O heteroatoms

for high-performance supercapacitor electrodes. Wood Sci Technol 57 (4), 879–901. https://doi.org/10.1007/s00226-023-01475-5.
[28] Zhou, Y., Qu, K., Zhang, L., Luo, X., Liao, B., 2021. Green fabrication of biodegradable cork membrane for switchable separation of oil/water mixtures. J Dispers Sci Technol 42 (2), 286–297. https://doi.org/10.1080/01932691.2019.1679641.
[29] Zhou, Y., Liao, B., Qu, K., Zhang, L., Ye, L., 2018. Cork membrane for efficient oil and water separation. Química Nova 41 (7), 810–813.
[30] Zhou, H.-Z., Jin, W.-L., Gan, X.-Q., Xin, C.-Y., Lv, Y.-Z., Xiao, M.-J., et al., 2024. Situ growth of Cofs within cork for oil–water separation: a comprehensive chemistry experiment for undergraduates. J Chem Educ 101 (10), 4306–4314. https://doi.org/10.1021/acs.jchemed.4c00426.
[31] Scalera, F., Monteduro, A.G., Quarta, A., Caputo, A., Pullar, R.C., Maruccio, G., et al., 2025. Cork-derived magnetic composites: a preliminary study. RSC Sustain 3 (2), 914–928.
[32] Scalera, F., Monteduro, A.G., Maruccio, G., Blasi, L., Gervaso, F., Mazzotta, E., et al., 2021. Sustainable chitosan-based electrical responsive scaffolds for tissue engineering applications. Sustain Mater Technol 28. https://doi.org/10.1016/j.susmat.2021.e00260.
[33] Seibert, D., Felgueiras, H.P., Módenes, A., Borba, F., Bergamasco, R., Homem, N.C., 2025. Application of cork as adsorbent for water and wastewater treatment using ciprofloxacin as pharmaceutical model. Int J Environ Sci Technol 22 (5), 3021–3038.
[34] Wang, Q., Luo, C., Lai, Z., Chen, S., He, D., Mu, J., 2022. Honeycomb-like cork activated carbon with ultra-high adsorption capacity for anionic, cationic and mixed dye: preparation, performance and mechanism. Bioresour Technol 357, 127363. https://doi.org/10.1016/j.biortech.2022.127363.
[35] Todescato, D., Hackbarth, F.V., Carvalho, P.J., Ulson de Souza, A.A., Ulson de Souza, S.M., Boaventura, R.A., et al., 2020. Use of cork granules as an effective sustainable material to clean-up spills of crude oil and derivatives. Environ Sci Pollut Res 27 (1), 366–378.
[36] Novais, R.M., Caetano, A.P.F., Seabra, M.P., Labrincha, J.A., Pullar, R.C., 2018. Extremely fast and efficient methylene blue adsorption using eco-friendly cork and paper waste-based activated carbon adsorbents. J Clean Prod 197, 1137–1147. https://doi.org/10.1016/j.jclepro.2018.06.278.
[37] Turco, A., Monteduro, A.G., Montagna, F., Primiceri, E., Frigione, M., Maruccio, G., 2023. The effect of synthetic conditions on piezoresistive properties of ultrasensitive carbon nanotube/PDMS 3D composites. Polymer 264, 125534. https://doi.org/10.1016/j.polymer.2022.125534.
[38] Turco, A., Monteduro, A.G., Montagna, F., Primiceri, E., Frigione, M., Maruccio, G., 2022. Does size matter? The case of piezoresistive properties of carbon nanotubes/elastomer nanocomposite synthesized through mechanochemistry. Nanomaterials 12 (21), 3741.
[39] Turco, A., Monteduro, A.G., Montagna, F., Primiceri, E., Frigione, M., Maruccio, G., 2022. Nanoarchitectonics of highly sensitive and with large working range 3D piezoresistive microporous foam based on carbon nanotubes and elastomer (https://doi.org/https://doi.org/). J Colloid Interface Sci 607, 1436–1445. https://doi.org/10.1016/j.jcis.2021.09.065.
[40] Scalera, F., Carbone, L., Bettini, S., Pullar, R.C., Piccirillo, C., 2020. Biomimetic calcium carbonate with hierarchical porosity produced using cork as a sustainable template agent. J Environ Chem Eng 8 (1), 103594. https://doi.org/10.1016/j.jece.2019.103594.
[41] Michalchuk, A.A., Friščić, T., 2025. Moving mechanochemistry forward: mechanochemistry and the non-covalent bond. RSC Mechanochem 2 (3), 333–335.
[42] Pullar, R.C., Novais, R.M., Caetano, A.P.F., Krishnakumar, K.A., Surendran, K.P., 2023. Ultra-light-weight microwave X-band EMI shielding or RAM material made from sustainable pyrolysed cork templates. Nanoscale 15 (39), 15982–15993. https://doi.org/10.1039/D3NR04411D.
[43] Kim, K.H., Cho, K.M., Kim, D.W., Kim, S.J., Choi, J., Bae, S.J., et al., 2016. The role of layer-controlled graphene for tunable microwave heating and its applications to the synthesis of inorganic thin films. ACS Appl Mater & Interfaces 8 (8), 5556–5562. https://doi.org/10.1021/acsami.5b11458.
[44] Turco, A., Primiceri, E., Frigione, M., Maruccio, G., Malitesta, C., 2017. An innovative, fast and facile soft-template approach for the fabrication of porous PDMS for oil–water separation. J Mater Chem A 5 (45), 23785–23793. https://doi.org/10.1039/c7ta06840a.
[45] Dudło, A., Michalska, J., Turek-Szytow, J., Kobyłecki, R., Zarzycki, R., Wichliński, M., et al., 2024. Humic substances sorption from wastewater on the biochar produced from the waste materials. J Environ Manag 370, 122366. https://doi.org/10.1016/j.jenvman.2024.122366.
[46] McCall, M.A., Watson, J.S., Tan, J.S.W., Sephton, M.A., 2025. Biochar stability revealed by FTIR and machine learning. ACS Sustain Resour Manag 2 (5), 842–852. https://doi.org/10.1021/acssusresmgt.5c00104.
[47] Johnson, L.M., Gao, L., Shields Iv, C.W., Smith, M., Efimenko, K., Cushing, K., et al., 2013. Elastomeric microparticles for acoustic mediated bioseparations. J Nanobiotechnol 11 (1), 22. https://doi.org/10.1186/1477-3155-11-22.
[48] Mo, S., Mei, J., Liang, Q., Li, Z., 2021. Repeatable oil-water separation with a highly-elastic and tough amino-terminated polydimethylsiloxane-based sponge synthesized using a self-foaming method. Chemosphere 271, 129827. https://doi.org/10.1016/j.chemosphere.2021.129827.
[49] Sun, X., Shi, K., Mo, S., Mei, J., Rong, J., Wang, S., et al., 2023. A sustainable reinforced-concrete-structured sponge for highly-recyclable oil adsorption. Sep Purif Technol 305, 122483. https://doi.org/10.1016/j.seppur.2022.122483.
[50] Ong, C.C., Sundera Murthe, S., Mohamed, N.M., Perumal, V., Mohamed Saheed, M. S., 2018. Nanoscaled surface modification of poly(dimethylsiloxane) using carbon nanotubes for enhanced oil and organic solvent absorption. ACS Omega 3 (11), 15907–15915. https://doi.org/10.1021/acsomega.8b01566.
[51] Zhang, W., Wang, J., Han, X., Li, L., Liu, E., Lu, C., 2021. Carbon nanotubes and polydopamine modified Poly(dimethylsiloxane) sponges for efficient oil–water separation. Materials.
[52] Liu, H., Sun, Y., Chen, Z., 2021. One-pot facile synthesis of PDMS/PDMAEMA hybrid sponges for surfactant stabilized O/W emulsion separation. Soft Matter 17 (41), 9363–9370. https://doi.org/10.1039/D1SM01061A.
[53] Qiu, S., Bi, H., Hu, X., Wu, M., Li, Y., Sun, L., 2017. Moldable clay-like unit for synthesis of highly elastic polydimethylsiloxane sponge with nanofiller modification. RSC Adv 7 (17), 10479–10486. https://doi.org/10.1039/C6RA26701G.
[54] Zhao, J., Chen, H., Ye, H., Zhang, B., Xu, L., 2019. Poly(dimethylsiloxane)/graphene oxide composite sponge: a robust and reusable adsorbent for efficient oil/water separation. Soft Matter 15 (45), 9224–9232. https://doi.org/10.1039/C9SM01984G.
[55] Sun, H., Zhu, Z., Liang, W., Yang, B., Qin, X., Zhao, X., et al., 2014. Reduced graphene oxide-coated cottons for selective absorption of organic solvents and oils from water. RSC Adv 4 (58), 30587–30591. https://doi.org/10.1039/C4RA03208J.
[56] Pan, Z., Guan, Y., Liu, Y., Cheng, F., 2021. Facile fabrication of hydrophobic and underwater superoleophilic elastic and mechanical robust graphene/PDMS sponge for oil/water separation. Sep Purif Technol 261, 118273. https://doi.org/10.1016/j.seppur.2020.118273.
[57] Prasanthi, I., Raidongia, K., Datta, K.K.R., 2021. Super-wetting properties of functionalized fluorinated graphene and its application in oil–water and emulsion separation. Mater Chem Front 5 (16), 6244–6255. https://doi.org/10.1039/D1QM00757B.
[58] Hu, Y., Jiang, Y., Ni, L., Huang, Z., Liu, L., Ke, Q., et al., 2023. An elastic MOF/graphene aerogel with high photothermal efficiency for rapid removal of crude oil. J Hazard Mater 443, 130339. https://doi.org/10.1016/j.jhazmat.2022.130339.
[59] Abdulhussein, A.T., Kannarpady, G.K., Ghosh, A., Barnes, B., Steiner, R.C., Mulon, P.Y., et al., 2018. Facile fabrication of a free-standing superhydrophobic and superoleophilic carbon nanofiber-polymer block that effectively absorbs oils and chemical pollutants from water. Vacuum 149, 39–47. https://doi.org/10.1016/j.vacuum.2017.11.028.
[60] Guo, Z., Long, B., Gao, S., Luo, J., Wang, L., Huang, X., et al., 2021. Carbon nanofiber based superhydrophobic foam composite for high performance oil/water separation. J Hazard Mater 402, 123838. https://doi.org/10.1016/j.jhazmat.2020.123838.
[61] Herren, B., Saha, M.C., Altan, M.C., Liu, Y., 2022. Funnel-shaped floating vessel oil skimmer with joule heating sorption functionality. Polymers.
[62] Sai, H., Fu, R., Xing, L., Xiang, J., Li, Z., Li, F., et al., 2015. Surface modification of bacterial cellulose aerogels' web-like skeleton for oil/water separation. ACS Appl Mater Interfaces 7 (13), 7373–7381. https://doi.org/10.1021/acsami.5b00846.
[63] Wu, Z.-Y., Li, C., Liang, H.-W., Chen, J.-F., Yu, S.-H., 2013. Ultralight, flexible, and fire-resistant carbon nanofiber aerogels from bacterial cellulose. Angew Chem Int Ed 52 (10), 2925–2929.
[64] Zhang, Z., Sèbe, G., Rentsch, D., Zimmermann, T., Tingaut, P., 2014. Ultralightweight and flexible silylated nanocellulose sponges for the selective removal of oil from water. Chem Mater 26 (8), 2659–2668. https://doi.org/10.1021/cm5004164.
[65] Abidli, A., Huang, Y., Park, C.B., 2020. situ oils/organic solvents cleanup and recovery using advanced oil-water separation system. Chemosphere 260, 127586. https://doi.org/10.1016/j.chemosphere.2020.127586.
[66] Abidli, A., Huang, Y., Cherukupally, P., Bilton, A.M., Park, C.B., 2020. Novel separator skimmer for oil spill cleanup and oily wastewater treatment: from conceptual system design to the first pilot-scale prototype development. Environ Technol Innov 18, 100598. https://doi.org/10.1016/j.eti.2019.100598.